Optogenetic countering of glial acidosis suppresses glial glutamate release and ischemic brain damage

Kaoru Beppu

Department of Physiological Sciences,

The School of Life Science,

The Graduate University for Advanced Studies

CONTENTS

1. Summary...……3
2. Introduction ……...6
3. Experimental procedures …….....10
3-1. Electrophysiology……...…10
3-2. pH imaging……12
3-3. Optogenetic mice……...13
3-4. *In situ* hybridization and immunohistochemistry……..13
3-5. *In vivo* optical stimulation of freely moving mice and *in situ* hybridization……14
3-6. HOKR experiments……...15
3-7. Immunogold electron microscopy of Mlc1-tTA::tetO-ArchT-EGFP mice……...15
3-8. Creation of cerebellar ischemia model and *in vivo* astrocytic ArchT-photoactivation..16
3-9. Immunohistochemistry for the evaluation of the infarct area……17
3-10. Statistical analysis……...18
4. Results……..19
4-1: Chapter 1. Astrocyte-photostimulation drives glutamate release and neuronal activity ……...19
4-1-1. Astrocyte-photostimulation drives neuronal activity…….....19
4-1-2. Astrocytic activation drives behavioral changes……20
4-1-3. Astrocyte-photostimulation induces glutamate release……..21
4-1-4. Astrocyte-photostimulation induces synaptic plasticity…….....22
4-2: Chapter 2. Acidification triggers glutamate release from astrocytes ..……..24
4-2-1. Mechanism for glutamate release by astrocytic ChR2 stimulation……....24
4-2-2. Glutamate release by astrocyte-photostimulation does not depend on calcium event…….....25
4-2-3. Acidification but not depolarization induces glutamate release…….26
4-3: Chapter 3. Acidification triggered glutamate release from astrocyte accelerates brain damage upon ischemia…...……...……30
4-3-1. Ischemia induces glutamate release and acidosis……..……30
4-3-2. Countering astrocytic acidosis inhibits neuronal damage……..……31
4-3-3. OGD response is different in the thalamus …….……...…….....34
5. Discussion……....36
5-1. Signaling pathway from astrocyte to neuron……36
5-2. Methods for evoking selective astrocyte-activation……..37
5-3. Mechanism of glutamate release from astrocytes……..…...38
5-4. pH dependent astrocytic glutamate release upon cerebellar ischemia…….…….38
5-5. Difference of astrocytic function in brain regions…….39
5-6. Astrocytic pH…….40
5-7. In the future..…….40
6. Acknowledgements……...41
7. References……....42
8. Figures and Figure legends (1-25) ……..……49

1. Summary

The brain is composed of many cells and it is considered that signals transmitted between these numerous cells are what underlie the basis of our mind and behavior. Glial cells comprise more or less half of the cells in the brain. However, active communication between neurons and glial cells has not been well understood as glial cells are mostly electrically silent. Here, I showed that astrocyte, one of the population of glial cells, can send information to neurons using glutamate as a transmitter. The mechanism of glutamate release was totally different from that in neurons, suggesting a role of astrocytes as a modulator of neuronal excitability and synaptic plasticity. I also found that the activity of astrocytes can run away and cause devastating effects on the homeostasis of the brain environment. A large contributor to the development of excitotoxicity upon ischemia was glutamate released from astrocytes, and this release was triggered by acidification in the astrocytes. Optogenetic countering of astrocytic acidosis was sufficient to suppress ischemic brain damage. These data suggest a two-sided nature of astrocyte; on one side, it can modulate behavior and learning in potentially physiological situations and, on the other side, it can have a destructive role upon pathology. In both cases, I showed that the glial cells are not silent and should not be a neglected population of cells in the brain.

In this thesis, I present data obtained using immunohistochemistry, electrophysiology, and behavioral studies. Controlling astrocytic activity at will was essential in understanding the function of astrocytes. To this end, I introduced transgenic mice which selectively express optogenetic tools such as chanelrhodopsin-2 (ChR2) and archaerhodpsin-T (ArchT) in astrocytes.

Astrocytes are known to maintain neuronal survival and functioning, such as

trophic support, uptake of glutamate, and removal of K^+ from extracellular space. Recent studies show that astrocytes exhibit dynamic and rapid activity in response to neuronal activity. However, whether astrocytes can send information back to neurons was largely unknown. This was because specific method to selectively stimulate astrocytes had not been available. However, recent technical advance in optogenetics enabled us to study the glia-to-neuron interaction.

To investigate whether astrocyte-to-neuron signaling exists, I established a transgenic mouse which expresses ChR2, a light gated cation channel, in astrocytes (Chapter 1). Optic fiber was placed on the cerebellum and astrocyte-photostimulation was delivered through the skull under free moving condition. Astrocyte-photostimulation induced expression of *c-fos*, suggesting that astrocyte activation could induce neuronal activity. In addition, cerebellar-dependent behavior and learning were also affected by astrocyte-photostimulation. This result suggests that astrocyte-to-neuron signaling exists and astrocytes can drive dynamic neuronal activity, which can alter the brain circuits' function.

I next searched for the signals that mediate astrocytic activity to neuronal excitation. Using cerebellar acute slice preparation of mice, I found that astrocyte-photostimulation leads to release of glutamate which activates AMPA-type glutamate receptor and metabotropic glutamate receptor mGluR1 expressed on neurons. As a result, long-term depression occurred in the cerebellar Purkinje cells, suggesting that synaptic plasticity was affected. This result suggests that the signal initiated from astrocyte is glutamate.

Next, the mechanism of glutamate release driven by astrocyte-photostimulation was investigated (Chapter 2). In neuron, glutamate release is known to be released by calcium-dependent vesicular release. However, I found that astrocyte-photostimulated

glutamate release was mediated by a quite different way. When ChR2 is opened by light application, proton influx occurs through ChR2 causing acidification within astrocytes. This proton elevation in astrocytes triggers anion channel opening and glutamate is released through this anion channel.

I next studied the astrocytic contribution to excitotoxicity because the form of astrocyte-to-neuron signaling that I found would likely manifest under pathological conditions (Chapter 3). Upon brain ischemia, two major events occur. One is acidosis, and the other is release of excess glutamate, which leads to excitotoxicity. However, it is not clear whether these two events are independent or related to each other. I hypothesized that the extreme acidification in astrocytes causes excess glutamate release. To verify this hypothesis, a tool to counter astrocytic acidification was required. Thus, I introduced a transgenic mouse line which expresses light sensitive proton pump, ArchT, in astrocytes. I found that countering of astrocytic acidification upon ischemia with ArchT-photostimulation dramatically inhibited astrocytic glutamate release and ischemic brain damage. This result suggests that acid-sensitive astrocytic glutamate release is the major cause of brain damage upon cerebellar ischemia.

In conclusion, my study suggests that astrocytes have a powerful role in regulating neuronal activity and brain healthiness. Further studies of the functions of astrocytic activity would likely elucidate previously unrecognized functions of the brain.

2. Introduction

To understand the brain function, researchers normally focused on neurons as brain function is thought to be regulated directly by neuronal activities. However, the brain is actually occupied mostly by another type of cells, glial cells. Their role was classically considered to be restricted to the maintenance of neuronal survival and functioning, such as trophic support, uptake of glutamate, and removal of K^+ from the extracellular space (Allen and Barres, 2009). However, recent studies show that one of the glial cells, astrocyte exhibits dynamic and rapid activities correlated with neuronal functions (Matsui and Jahr, 2003). Astrocytes respond to neuronal activity by increasing intracellular calcium (Piet and Jahr, 2007) and altering morphology of their fine processes (Iino et al., 2001). Astrocytic activity also correlates with behavior and cognitive functions (Nimmerjahn et al., 2009; Schummers et al., 2008). However these are only studies of correlation. We do not know whether the activity of astrocytes has any significance in the function of the brain. If signaling pathway leading from astrocytes to neurons does not exist, the activity of astrocytes would have no role in our behavior and mind. Neuronal network and astrocytic network are not likely to be independent parallel networks; thus, I decided to seek the presence and significance of the dynamic interplay between the two.

To study the astrocyte-to-neuron interaction, a method to selectively stimulate astrocytes is required. Electrical or mechanical stimulations (Angulo et al., 2004) can evoke astrocytic depolarization and calcium increase. However these methods inevitably stimulate both neuron and glia. Direct intracellular stimulation of astrocyte (Jourdain et al., 2007) is also difficult as the input resistance of these cells is low and the

depolarization generated by the somatic electrode will not propagate through the complex astrocytic structures. Uncaging of caged Ca^{2+} within astrocytes is possible (Fellin et al., 2004; Perea and Araque, 2007). However, caged Ca^{2+} must be selectively loaded into astrocyte via patch pipette and loading more than a couple of cells would be technically difficult. If the coordinated activity of many astrocytes is required to induce an effect, this would be difficult to assess with the uncaging methods. Activation of group 1 metabotrophic glutamate receptors (mGluRs) can increase intracellular Ca^{2+} concentration in numerous astrocytes (Fellin et al., 2004). However, even with local application of mGluR1 agonist, neuronal group 1 mGluRs would also likely be activated. In addition, a report (Sun et al., 2013) shows that astrocytic Ca^{2+} signaling through mGluRs is undetectable in adult rodents. Astrocytes which transgenically express MAS-regulated G protein-coupled receptor member A1 (MRGA1) could be selectively activated by using an agonist that does not bind endogenous receptors in the brain (Fiacco et al., 2007). This would be an useful method, however application to *in vivo* study may not be straightforward as delivery of the drug may not be simple, and the cessation of the stimulus would be slow and depend on the loss of the agonist via diffusion. In addition, the reports (Agulhon et al., 2010; Fiacco et al., 2007) shows that selective astrocytes stimulation with their methods has no effect on neuronal activity, which challenges the idea that Ca^{2+} is the trigger of astrocyte-to-neuron signaling pathway.

Here, I used optogenetics to circumvent above problems (Fenno et al., 2011). An important advantage of the optogenetic tools, such as channelrhodopsin-2 (ChR2), a light-gated non-selective cation channel, is its cell-type specificity. I introduced a transgenic mouse line in which highly-sensitive mutant (C128S (Berndt et al., 2009)) of

ChR2 was selectively expressed in astrocytes including Bergmann glial cells (BGs) using the tetracycline transactivator (tTA)-tet operator (tetO) system (Tanaka et al., 2012). Using these mice, I found that astrocyte-photostimulation induced neuronal activity, synaptic plasticity, and behavioral modulations, which were mediated by astrocytic glutamate release (Chapter 1).

I also show that intracellular acidification is enough to induce glutamate release, and depolarization or calcium is not the trigger for the glutamate release induced by ChR2-photostimulation (Chapter 2).

Acid-triggered astrocytic glutamate release may operate in physiological situation to set the tone of neuronal activity. However to focus on this form of astrocyte-to-neuronal activity, I turned to pathological condition where this signaling would likely manifest most. I show that ischemic acidosis is the direct trigger for astrocytic excess glutamate release (Chapter 3).

In all of the above studies, I focused on one type of astrocytes in the cerebellum, Bergmann glial cells, because of the close morphological apposition of these astrocytes and neuronal elements, which suggests that, if there is any commitment of astrocytic activities in physiological or pathophysiological circumstances, it could manifest most in the cerebellum. However, regional differences should be taken account as pH sensitive ATP release from astrocytes occurs in the brainstem but not in the cortex (Gourine et al., 2010; Kasymov et al., 2013). Thus, I performed several experiments by using thalamic brain slices to investigate whether acid sensitive glutamate release occurs also in thalamic astrocytes upon ischemia. Thalamus is the region where it tends to be exposed to ischemic stress due to the morphological disposition of the brain blood vessels. Preliminary findings suggest that pH-dependent astrocytic glutamate release

does also occur in the thalamus but not as extensively as in the cerebellum. Factors other than glutamate release may mediate excitotoxicity in the thalamus but, interestingly, this was also inhibited by optogenetic activation of a proton pump. Identification of other pH dependent molecules will be required to further address clinically relevant issues.

3. Experimental procedures

3-1. Electrophysiology

Acute parasagittal cerebellar slices (250 μm) from mice (P17–24) were prepared in ice-cold solution containing (in mM) 119.0 NaCl, 2.5 KCl, 0.1 $CaCl_2$, 3.2 $MgCl_2$, 1.0 NaH_2PO_4, 26.2 $NaHCO_3$, 11.0 glucose, 3.0 myo-inositol, 0.5 ascorbic acid, and 2.0 Na-pyruvate (saturated with 95% O_2, 5% CO_2) and incubated in solution with $CaCl_2$ and $MgCl_2$ concentrations substituted to 2.0 and 1.3 mM, respectively, at 32°C for 30 min and then stored and used for recordings at room temperature (22~25°C), except for the recordings in Fig. 20A which were done at physiological temperature (33~35°C). A slice was transferred to a submerged-type recording chamber for the experiment and continuously superfused.

To simulate energy deprivation upon brain ischemia, glucose was omitted and superfusate bubbled with 95% N_2, 5% CO_2 was used (oxygen and glucose deprivation; OGD).

Cells were visualized using a ×60 water immersion objective on an upright microscope equipped with infrared-DIC. Whole-cell recordings were made with patch electrodes with resistances of 2–4 MΩ. Pipette solution (PS) with one of the following compositions was used. PS1 (in mM): 35 CsF, 100 CsCl, 10 HEPES, 10 EGTA; PS2: 145 CsCl, 2 $MgCl_2$, 10 HEPES, 2 Na_2ATP, 0.3 NaGTP, 5 Na-phosphocreatine, 10 Cs_2EGTA; PS3: 142 K-gluconate, 2 KCl, 10 HEPES, 0.5 EGTA, 4 $MgCl_2$, 4 Na_2ATP, 0.5 NaGTP (pH = 7.2 with CsOH titration for PS1 and PS2, and with KOH titration for PS3). PS1 was used for most of the voltage clamp experiments, PS2 for the OGD experiments and long term recordings under voltage clamp condition (Vh = –70 mV,

~80% series resistance compensation), and PS3 for the current clamp experiments (junction potential of –15.4 mV was corrected for these recordings). Inward current left in the presence of GluR/T blocker, DIDS, or during astrocytic ArchT-photoactivation was divided by the maximum inward current caused by the OGD to calculate the blocking effect (Fig. 17D, 20A, 21A and 21C). To manipulate intracellular pH buffering capacity (Fig. 14 and 15), $NaHCO_3$ was omitted and HEPES was used as the pH buffer in the external solution, which contained (in mM) 119.0 NaCl, 2.5 KCl, 2 $CaCl_2$, 1.3 $MgCl_2$, 1.0 NaH_2PO_4, 5 HEPES, 11 glucose, 30 sucrose, 3.0 myo-inositol, 0.5 ascorbic acid, and 2.0 Na-pyruvate (pH = 7.4 with NaOH, 300 mOsm with sucrose, and saturated with 100% O_2) (Zhang et al., 2010). To investigate H^+ permeability of ChR2(C128S) (Fig. 13A), extracellular and intracellular cations were mostly replaced with N-Methyl-D-glucamine (NMDG). External solution contained (mM): 147.8 NMDG, 2.0 $BaCl_2$, 1.3 $MgCl_2$, 11 Glucose, 20 HEPES (pH = 7.4, 5.0 and 9.0 with TEA-OH, 300 mOsm, saturated with 100% O_2) and intracellular PS4 (in mM): 128 NMDG, 128 HCl, 20 HEPES, 10 EGTA (pH = 7.2 with CsOH) was used.

Photostimulation was delivered to the slices from the epifluorescence port and through the ×60 objective. Light source with colors, blue (475/28 nm, power below the objective lens 0.9 mW, density (power/area) 7 mW/mm^2) and yellow (575/25 nm, 1.4 mW, 11 mW/mm^2) was used. Photostimulation consisting of a sequence of blue and yellow light was applied for ChR2(C128S) activation and only yellow light for the ArchT activation. To electrically stimulate parallel fibers, a theta glass pipette filled with bath solution was used and brief electrical pulses were given using a constant voltage-isolated stimulator. Stimulus strength was adjusted so that the PC EPSC amplitude did not exceed 400 pA. Glutamate receptor sensitivity was assessed by puff

application (2.5–10 psi) of glutamate (200 μM) for 10 s every 2 min. Glutamate was diluted in HEPES buffer solution (pH = 7.4, 300 mOsm). Intracellular acidification was evoked by puff application of Na-acetate (20 mM) for 10 s. Na-acetate was added to our normal ACSF with TTX, Cd^{2+}, and PIC (saturated with 95% O_2, 5% CO_2). Cellular depolarization was induced by puff application of high K^+ for 300 ms every 1 min. The high K^+ solution contained 50 mM KCl replaced with the same amount of NaCl in the HEPES buffer solution (pH = 7.4, 300 mOsm).

The sources of the chemicals are as follows: tetrodotoxin (TTX) and 2,3-dioxo-6-nitro-1,2,3,4-tetrahydrobenzo[f]quinoxaline-7-sulfonamide (NBQX) were from Ascent Scientific; $CdCl_2$, picrotoxin (PIC), and 4,4'-diisothiocyanostilbene-2,2'-disulphonic acid (DIDS) were from Sigma; DL-threo-β-benzyloxyaspartic acid (TBOA), D-(2R)-amino-5-phosphonovaleric acid (D-AP5), 1-(4-Aminophenyl)-3-methylcarbamyl--4-methyl-3,4-dihydro-7,8-methylenedioxy-5H-2,3-ben-zodiazepine hydrochloride (GYKI), and (S)-(+)-α-Amino-4-carboxy-2-methylbe-nzeneacetic acid (LY367385) were from Tocris Cookson; BAPTA-AM was from Invitrogen; Carbenoxolone (CBX) were from Sigma; 5-nitro-2-(3-phenylpropyl amino) benzoic acid (NPPB) was from Biomol.

3-2. pH imaging

Cells were loaded with a pH indicator by local puff application of SNARF-5F AM (200 μM) for 5 min at 10 psi to the acute slices. One of the technical reasons for selecting the cerebellum for the research was because of the ease to identify BG cell bodies based on its morphological characteristics. SNARF-5F was excited with 810 nm two-photon laser and fluorescence was detected using two emission filters (586/20 nm

and 650/60 nm) and the fluorescence ratio ($R_{650/586}$) was calculated. For Fig. 19D, only single emission wavelength (650/60 nm) was measured, as the space was occupied with a mechanical shutter that protects the photomultiplier tube upon ArchT-photoactivation. ΔF/F was calculated for these recordings. Z-stacks with 1 μm steps was obtained and the average fluorescence intensity from 1 to 3~5 optical slices that captured the full extent of the cell soma of interest was measured. For the ChR2(C128S) photoactivation, 473 nm laser was focally applied to the soma of a BG through the objective lens and two-photon pH imaging was obtained before and after the photoactivation. For the ArchT-photoactivation, diffuse 575/25 nm light was applied through the condenser lens. SNARF-5F AM was obtained from Invitrogen.

3-3. Optogenetic mice

Details are described elsewhere (Tanaka et al., 2012; Tsunematsu et al., 2013). tetO-ChR2(C128S)-EYFP β-actin gene locus knockin mice, tetO-ArchT-EGFP β-actin gene BAC transgenic mice, and Mlc1-tTA BAC transgenic mice were used. Bigenic mice were prepared by crossing Mlc1-tTA line expressing tTA under the control of Mlc1 promoter, which is selective for astrocytes (Sasaki et al., 2012; Tanaka et al., 2010) with either of the tetO lines. Another technical reason for selection of the cerebellum for my study was because both transgenic mice had highest expression of ChR2 and ArchT in cerebellar astrocytes. Especially ChR2 are known to have very low single channel conductance; thus, high expression was preferred to ensure consistent optical manipulation of cell activity.

3-4. *In situ* hybridization and immunohistochemistry

To confirm the cell-type specific expression of *tTA*, *in situ* hybridization for *tTA* was combined with immunohistochemistry for BLBP, calbindin-D, and NeuN. Detailed methods for *in situ* hybridization are described elsewhere (Ma et al., 2006). In brief, cryosections from 4% paraformaldehyde perfused brains were hybridized to digoxigenin-labeled *tTA* cRNA probes. Individual marker proteins were labeled with anti-BLBP antibody (rabbit monoclonal antibody, gift from Dr. M. Watanabe), anti-GFAP (rabbit polyclonal antibody, DakoCytomation), anti-Calbindin-D antibody (mouse monoclonal antibody, DBS), and anti-NeuN antibody (mouse monoclonal antibody, CHEMICON). Following the incubation of biotin-tagged secondary antibody, VECTASTAIN Elite Kit (Vector Lab) was used for the color development with 3,3'-Diaminobenzidine (DAB).

3-5. *In vivo* optical stimulation of freely moving mice and *in situ* hybridization

Mice over 12 weeks were used for the *in vivo* experiments. Blue (445 nm) and yellow (589 nm) lights were generated by laser diodes and applied through a plastic optical fiber (0.75 mm diameter). An optical swivel (Lucir) was used for unrestrained *in vivo* photostimulation. Blue and yellow light power intensities at the tip of the plastic fiber were 1.3 mW and 0.9 mW, respectively. Under anesthesia with 50 mg/kg pentobarbital, the plastic optical fiber was placed on the skull just above the cerebellum, 6.0 mm posterior to the bregma and fixed using dental cement. After at least a couple of days from the surgery, the photostimulation experiment was executed. The mice were sacrificed after 10 min from the photostimulation and *in situ* hybridization for *c-fos* and *c-fms* was performed as described previously (Ma et al., 2006). In brief, digoxigenin-labeled *c-fos*, *c-fms*, and *GAD67* cRNA probes (Pizoli et al., 2002) were

hybridized to sections, NBT/BCIP compounds (Roche) were used for color development, and nuclear fast red (Vector Lab) was used for counterstaining.

3-6. HOKR experiments

For the surgery, the mice were anesthetized with 1.5% isoflurane. Two holes (~1.0 mm diameter) were drilled bilaterally in the cranium, 6.0 mm posterior, 2.7 mm lateral to the bregma. Plastic optical fibers (0.5 mm diameter) with the ends entering the brain cut at a 45 degree angle were inserted 1.5 mm deep (Fig. 4A). The fiber was fixed onto the skull with dental cement. A flat head screw (6 mm head, 7 mm length) was also fixed onto the skull with dental cement on the midline between the bregma and lambda. After a couple of days from the surgery, the head of the unanethesized mice was fixed to a home-made device using the above screw and nuts. Lights from blue and yellow LEDs (470 and 590 nm) were delivered to the open ends of the optical fibers (power intensity at the output tip, ~0.6 and ~0.6 mW, respectively).

A sheet of paper with checker pattern was placed semi-circularly (radius 32 cm) surrounding the head-fixed mouse and oscillated horizontally and sinusoidally. The screen movement was 17 deg and the cycle was set at 3.0–5.0 s. The eye image was captured using a CCD camera sensitive to infrared light. The pupil location and size were calculated with the method described previously (Sakatani and Isa, 2004) and with the FIJI software (GPL).

3-7. Immunogold electron microscopy of Mlc1-tTA::tetO-ArchT-EGFP mice

Deeply anaesthetized mice were transcardially perfused through the ascending aorta with 25 mM phosphate-buffered saline (PBS, pH 7.4) for 1 minute followed by a

fixative containing 4% paraformaldehyde (PFA), 0.05% glutaraldehyde and 15% saturated picric acid made up in 0.1 M phosphate buffer (PB; pH 7.4) for 12 minutes (total 50 ml). After perfusion, brains were quickly removed from the skull, washed briefly with PB and parasagittally sectioned at 50 μm with a microslicer (Linear 7 Pro, Dosaka). These sections were cyroprotected with 30% sucrose in PB and freeze-thawed. Subsequently, sections were blocked for 45 minutes in 10% normal goat serum (NGS) in Tris-buffered saline (TBS, pH 7.4) and incubated overnight at 4 ^{o}C in primary antibody (1 μg/ml mouse anti-GFP antibody, Clone mFX73, Wako) made up in TBS containing 1% NGS. After washing, the sections were incubated with 1.4 nm gold-coupled (Nanoprobes Inc., Stony Brook) anti-mouse secondary antibody diluted in TBS at a ratio of 1:100 overnight at 4^{o}C. After washing, the sections were postfixed in 1% glutaraldehyde for 10 minutes, followed by gold enhancement of the immunogold particles using a gold enhance-EM kit (Nanoprobes Inc.). Sections were then postfixed with 1% osmium tetroxide for 40 minutes, en bloc counterstained with 1% uranyl acetate for 30 minutes, and dehydrated in graded ethanol series followed by propylene oxide. The sections were infiltrated overnight at room temperature in Durcapan resin (Sigma-Aldrich) and transferred to glass slides for flat embedding. After resin curing at 60 ^{o}C, the trimmed tissues from the region of interest were re-embedded in Durcapan resin blocks for ultrathin sectioning. Serial 70 nm thick sections were cut from the surface (within 3 μm depth) of the samples and were collected in pioloform-coated single slot copper grids. Images were captured by a CCD camera that was connected to a JEM1011 transmission electron microscope (JEOL Co., Akishima).

3-8. Creation of cerebellar ischemia model and *in vivo* astrocytic

ArchT-photoactivation

Mice (over 7 weeks old) were anesthetized with 1.5% isoflurane and placed in a stereotaxic frame. Circular craniotomy (~1.0 mm diameter) was made over the cerebellum at 6.0 mm posterior to the bregma. A photosensitive dye, rose bengal (0.02 mg/g body weight), was administrated through the left carotid artery (Watson et al., 1985) and 5 min after the injection, the dye was excited (center 575 nm, width 25 nm, power 12.9 mW) for 4-5 min via an optical fiber placed just above the craniotomy. As all *in vivo* experiments were done using Mlc1-tTA::tetO-ArchT mice, the procedure for the artificial thrombosis creation likely photoactivated the glial ArchT as well; however, this is true for both the control group and for the group that experienced subsequent intermittent glial ArchT-photoactivation (1s light on, 1 s light off cycle for 2.5 hours), which started after 30 min from the photothrombosis. The mice were sacrificed after 3 hours from the photothrombosis and used for immunohistochemical analysis.

3-9. Immunohistochemistry for the evaluation of the infarct area

Mice were anesthetized with 50 mg/kg pentobarbital and perfused transcardially with cold 4% PFA in 25 mM PBS. The brain samples were postfixed with 4% PFA overnight at 4°C. The fixed brains were rinsed 3 times with PBS and parasagittal cerebellar slices (100 μm) were prepared and permeabilized in PBS with 0.3% Triton X-100 and 5 % NGS at room temperature for 60 min. The samples were then incubated with a primary antibody against Calbindin-D (1:500; mouse monoclonal antibody, DBS) in PBS with 0.3% Triton X-100 and 5% NGS overnight at 4°C. Following this antibody incubation, the slices were rinsed 3 times with PBS and then incubated with secondary anti-mouse IgG Alexa-594 (1:1,000; Invitrogen) in PBS with 5% NGS for 2 hours at

room temperature.

To assess neuronal loss and infarct area, brain sections were scored (from 1, mild to 4, very severe) in a blinded manner based on the loss of PC fraction and the spread of degenerated area. The region approximately 300 μm from the center of the illuminated surface was analyzed. The criteria for the scoring are shown in Fig. 24B. The Wilcoxon rank-sum test was used to compare score distributions between the control and the intermittent glial ArchT-photoactivated groups.

3-10. Statistical analysis

Electrophysiological and SNARF-5F imaging data were analyzed with AxoGraphX and ImageJ. Statistical analysis was conducted by Excel and SPSS. Data are shown as mean ± s.e.m.

4. Results

4-1. Chapter 1:
Astrocyte-photostimulation drives glutamate release and neuronal activity

4-1-1. Astrocyte-photostimulation drives neuronal activity

To selectively stimulate the astrocyte, Dr. Tanaka KF (Keio Univ.) generated two lines of mice (Tanaka et al., 2012); one in which the expression of tetracycline-controlled tTA is driven by megalencephalic leukoencephalopathy with subcortical cysts 1 (Mlc1)-promoter, which has been proven to be astrocyte specific (Schmitt et al., 2003), and the other in which tetO is connected to the expression of C128S mutant of ChR2 (Berndt et al., 2009) fused with enhanced yellow fluorescent protein (EYFP). By obtaining bigenic (Mlc1-tTA::tetO-ChR2(C128S)-EYFP) mice, strong EYFP expression was found in Bergmann glial cells (BGs) in the cerebellum (Fig. 2A). A point mutation (C128S) of the ChR2 causes prominent increases in photosensitivity as well as alteration in the photocycle, enabling a step-like control of the photocurrent by blue and yellow light (Berndt et al., 2009). To validate the selective expression of ChR2(C128S) in astrocytes, whole-cell patch clamp recordings were performed in acute cerebellar slices in the presence of a cocktail of pharmacological agents which silence neuronal activity (Fig. 2B). Current responses to photostimulation were detected only in BGs (n = 24), but not in Purkinje cells (PCs) (n = 10), granule cells (GCs) (n = 10), and stellate/basket cells (SC/BCs) (n = 11). Furthermore, simultaneous *in situ* hybridization for *tTA* and immunohistochemistry for brain-lipid-binding protein (BLBP) confirmed the specificity of transgene expression in

BGs (Fig. 2C). These results demonstrate that, in our transgenic mice, ChR2 expression is restricted to astrocytes.

My first aim was to assess whether astrocyte-to-neuron communication could be elicited by photostimulation of astrocytes. To evaluate this *in vivo*, an optic fiber was placed just on the skull above the cerebellum of the transgenic mouse (Fig. 3A). While the mouse moved freely in a home cage, a single photostimulation (200 ms blue and 200 ms yellow with an interval of 500 ms) was applied (Fig. 3B). After sacrificing the mouse, *in situ* hybridization for *c-fos* mRNA, an immediate early gene as a marker of neuronal activation, was performed (Fig. 3C). At the region directly beneath the optic fiber, strong *c-fos* expression was observed in PCs, SC/BCs, and GCs. Expression of *c-fos* was not observed in non-photostimulated ChR2(+)-mice or in photostimulated ChR2(−)-mice (Fig. 3D and E). The microglial cell distribution and morphology appeared normal (Fig. 3F).

4-1-2. Astrocytic activation drives behavioral changes

I next investigated whether signals initiated from astrocytes could propagate through the neuronal network and drive behavioral responses *in vivo*. Photostimulation was applied through optical fibers inserted close to the cerebellar flocculus region (Fig. 4A) and an induction of *c-fos* mRNA in a subset of PCs, GCs and SC/BCs was observed by the astrocytic-photostimulation (Fig. 4B). In this condition, I assessed the effect of astrocyte-photostimulation on the eye movement (Fig. 4C). Amplitude increase of the horizontal optokinetic reflex (HOKR) upon repetitive visual stimulation has been shown to be controlled by the activity of the flocculus (Katoh et al., 1998; Schonewille et al., 2006). Astrocyte-photostimulation was done while HOKR training and perturbation of

the smooth eye pursuit of the visual stimulation was evoked every time the photostimulation was applied (Fig. 4D). In addition, pupil dilation was also evoked (Fig. 4E and F); which is in agreement with the fact that the cerebellum and the deep cerebellar nulei modulate pupil size (Ijichi et al., 1977). After the pupil area came back close to the basal value (Fig. 4F), the HOKR amplitude was measured and an increase compared to the baseline was observed (Fig. 4E and G). This effect lasted for a couple of minutes, probably due to the prolonged modulation of neuronal circuit by the powerful activity of astrocytes. Despite of the perturbation of eye movement as well as the transient increase in the HOKR amplitude, HOKR amplitude increase after 1 hour continuous visual training was observed in most mice as in the ChR2(−)-mice (Fig. 4H and I).

4-1-3. Astrocyte-photostimulation induces glutamate release

Even though only the astrocyte was photostimulated in the absence of pharmacological agents, *c-fos* was elevated in neurons. While elevated K^+ could be one of the mechanisms underlying neuronal excitation, I examined whether any other substance is released following astrocyte-photostimulation. The receptors expressed on PC membrane were used as biosensors to detect the released substance in acute cerebellar slices. Neuronal transmitter release was inhibited by applying 0.5 μM tetrodotoxin (TTX) and 100 μM Cd^{2+}, to block action potentials and voltage-gated Ca^{2+} channels, respectively. Since astrocyte-photostimulated PC-currents remained intact in the presence of 100 μM picrotoxin (PIC) (Fig. 5A), GABA is not likely to be the transmitter (Lee et al., 2010). Thus, PIC was also added to inhibit neuronal $GABA_A$ mediated response, and focused on excitatory gliotransmitter. In this condition,

astrocyte-photostimulation produced an inward current in the recorded PC (Fig. 5B), suggesting that the receptors on PCs were activated. I next sought to identify the excitatory transmitter. Application of AMPAR antagonist, 10 μM NBQX (Fig. 5B) or 100 μM GYKI53655 (Fig. 5C), entirely abolished the astrocyte-photostimulated PC-current. The kinetics of the slowly developing PC-current was mimicked by local pressure injection (puff) of exogenous glutamate (Fig. 5D). Addition of 100 μM TBOA, glutamate transporter blocker, caused a significant increase in the amplitude of the astrocyte-photostimulated PC-current (Fig. 5E). Glutamate transporter blockade likely increased the concentration of glutamate reaching the AMPARs. Taken together, these lines of experiments demonstrate that astrocyte-photostimulation causes releases of glutamate, and the released glutamate reaches the low affinity PC AMPARs (EC_{50} = 432 μM (Hausser and Roth, 1997)) at a sufficient concentration.

4-1-4. Astrocyte-photostimulation induces synaptic plasticity

The released glutamate can activate not only AMPARs but also metabotropic glutamate receptors type 1 (mGluR1), which are expressed on the peripheral of the PC spines and dendrites (Baude et al., 1993), but have not been detected on cerebellar astrocytic cell membrane (Lopez-Bendito et al., 2001). Activation of mGluR1 is essential for inducing synaptic plasticity at PF-PC synapses and for coordinated motor behavior (Aiba et al., 1994). BG processes are situated immediately adjacent to the mGluR1 on PCs, which raises a possibility that glutamate released from astrocyte-photostimulation could induce changes in neurotransmission from PFs to PCs. To test this, we examined the effect of the astrocyte-photostimulation on PF-PC excitatory postsynaptic currents (EPSCs) (Fig. 6A). A single 10 s-photostimulation

induced long-term depression (LTD) of PF-PC EPSCs (Fig. 6A and B). Application of an mGluR1 antagonist, 100 μM LY367385, blocked the LTD (Fig. 6B, C). No change in the input resistance of PCs was detected after photostimulation. The photostimulation did not significantly alter the EPSC paired-pulse ratio (Fig. 6D), implying that presynaptic components were not affected by the photostimulation.

In this chapter, I showed that astrocyte-photostimulation induced neuronal activity and glutamate released from astrocytes activates AMPARs and mGluRs on PCs. Signals initiated from astrocytes propagate through the neuronal network and cause behavior and learning perturbation (Fig. 7). These results suggest a potential role of astrocytes in actively participating in the information processing in the brain.

4-2. Chapter 2:

Acidification triggers glutamate release from astrocytes

4-2-1. Mechanism for glutamate release by astrocytic ChR2 stimulation

In chapter 1, I found that glutamate mediates astrocyte-to-neuronal signaling. In this chapter, I will investigate the mechanism of glutamate release induced by the astrocyte-photostimulation (Fig. 8). Over 50 years of the research, starting from the studies of neuromuscular junction by Katz and Miledi, strongly supports the idea that neurotransmitter release from neurons is mediated by calcium dependent exocytosis of synaptic vesicles. Recent studies also imply that glutamate is released from astrocytes by exocytosis (Jourdain et al., 2007); however most electron microscopic studies failed to demonstrate the presense of synaptic-vesicle-like structures in astrocytes. Several pathways for glutamate release from astrocytes have been suggested (Hamilton and Attwell, 2010): these include (i) anion channel opening, (ii) functional unpaired connexin hemichannel, and (iii) reversal of uptake by Na^+-dependent glutamate transporters. Glutamate is an anion. An anion channel blocker, DIDS, has been shown to block glutamate release from astrocytes (Liu et al., 2009). 1 mM DIDS abolished the astrocyte-photostimulated PC-current (Fig. 9A), whereas no change in the current responses of PCs to exogenous puff application of glutamate was observed in the presence of DIDS (Fig. 9B). The BG photocurrent remained intact (Fig. 9C). Another type of anion channels blocker NPPB (100 μM) did not alter the astrocyte-photostimulated PC-current (Lee et al., 2010) (Fig. 9D). In the presence of 100 μM CBX, one of the most widely used gap junction/hemichannel blocker, the current response remained normal (Fig. 9E), ruling out the contribution of hemichannel

opening. It has been suggested that the reversal of glutamate transporter can be blocked by extracellular TBOA (Phillis et al., 2000). However, TBOA failed to inhibit astrocyte-photostimulated PC-current but rather enhanced it (Fig. 5E). This enhancement was not unexpected, because TBOA blocks glutamate uptake as well. If TBOA cannot block glutamate release, then the released glutamate would linger in the extracellular space for longer because the uptake is also inhibited. Tetanus toxin or Bafilomycin A pretreatment, which is reported to disrupt vesicle fusion or vesicular filing of glutamate, respectively, failed to abolish neuronal synaptic release in our condition, possibly due to the rather developed age of animals that I used which may preclude the penetration of these molecules; therefore, I was unable to assess the role of vesicle exocytosis mediating gliotransmitter release. These results suggest that glutamate release by astrocyte-photostimulation is likely via anion channels not sensitive to NPPB but sensitive to DIDS (Cavelier and Attwell, 2005).

4-2-2. Glutamate release by astrocyte-photostimulation does not depend on calcium event

I next investigated the pathway leading from astrocyte-photostimulation to anion channel opening. Calcium increase is known to be pivotal in many cellular functions and reports suggest that glutamate release from astrocytes depends on calcium (Halassa and Haydon, 2010); however, importance of calcium has been questioned in some studies (Fiacco et al., 2007; Agulhon et al., 2010). Here, I investigated whether calcium mediates astrocyte-photostimulated glutamate release. To inhibit calcium influx from the extracellular space, Ca^{2+} was omitted and 5 mM EGTA was added to the extracellular solution. The astrocyte-photostimulated PC-current remained uninhibited

in this condition (Fig. 10A), suggesting that calcium influx is not the trigger for astrocyte-photostimulated glutamate release. It is still possible that intracellular Ca^{2+} increase could occur via Ca^{2+} release from internal stores. To evaluate this possibility, intracellular Ca^{2+} was strongly buffered with BAPTA-AM. Although BAPTA-AM was sufficient to strongly suppress neuronal synaptic release of glutamate (Fig. 10B), it did not significantly alter astrocytic ChR2-photoactivated PC-currents (Fig. 10C). It still remains possible that coupling between Ca^{2+} source and glutamate release mechanisms is even tighter in astrocytes than in synapses. However, the Ca^{2+} permeability of ChR2 is very low unless it is specifically modified (Kleinlogel et al., 2011; Li et al., 2012). Together with this ChR2 property and our results (Fig. 10A, C), I conclude that Ca^{2+} influx through these channels is not likely to be sufficient to drive astrocyte-photostimulated glutamate release (Woo et al., 2012).

4-2-3. Acidification but not depolarization induces glutamate release

I next searched for the trigger other than calcium. ChR2 is a light-sensitive cation channel and it is usually considered as a tool to optically excite cell activity via membrane depolarization. It is possible that depolarization directly triggers glutamate release (Yaguchi and Nishizaki, 2010). To simply investigate depolarization as the trigger for astrocytic glutamate release, I examined the effect of puff application of high concentration of K^+. High K^+ application alone would depolarize neuron as well and cause neuronal transmitter release. Thus, high K^+ was applied in the presence of TTX and Cd^{2+} to block neuronal transmitter release. PIC was also added to block $GABA_A$ receptors and focus on the excitatory pathway. High K^+ application caused BG depolarization. Under voltage-clamp mode, inward current was recorded in PCs in

response to the high K^+ puff. This response is likely due to the influx of K^+ through leak K^+ conductance of PCs at resting potentials. The current recorded from PCs was not altered by application of GYKI or NBQX (Fig. 11A). Thus, glutamate is not likely to be released as a consequence of BG depolarization or by the presence of high extracellular K^+ (Fig. 11).

Contrary to other excitatory channels such as Na^+ channels or ionotropic glutamate receptor channels, ChR2 has much more permeability to H^+ than Na^+ (Nagel et al., 2003). Thus, proton influx can be the direct trigger for astrocytic glutamate release. To simply test whether H^+-triggered glutamate release occurs, a method to induce intracellular acidification was employed which was to locally pressure (puff) apply a weak membrane permeable acid, acetate. In the presence of TTX, Cd^{2+} and PIC, acetate application did not induce depolarization of BGs but did evoke a slow inward current in PCs, which was not detected in the presence of GYKI (Fig. 11B). This result suggests that acetate-induced intracellular acidification evoke non-synaptic glutamate release. However in this experiment, not only astrocytes but also other cells are acidified. Thus, using ChR2 is currently the only method to specifically acidify astrocytes.

To evaluate whether astrocytes are truly acidified upon ChR2 activation, first I examined whether proton influx occurs through ChR2 by measuring photocurrents from BGs with intracellular and extracellular cations mostly replaced with N-Methyl-D-glucamine (NMDG), a cation with little permeability to ChR2; thus, the only cation left permeable was proton (Fig. 13A). Decreasing pH means increasing proton concentration. Decreasing the external pH from 7.4 to 5.0 enhanced the photocurrent, whereas increasing the pH from 7.4 to 9.0 reduced it. These data suggest that our C128S modified ChR2 expressed in BGs are also permeable to proton, although

it is possible that ChR2 channel opening itself could be regulated by external pH. To verify proton influx through ChR2(C128S) in normal intracellular and extracellular solutions, pH imaging was performed and BG acidification by ChR2(C128S) photoactivation was confirmed (Fig. 13B). These data demonstrate that our C128S modified ChR2 expressed in BGs are also permeable to proton, increasing the possibility that proton influx directly triggers astrocytic glutamate release (Fig. 13C, D).

To positively identify H^+ as the trigger of the release, I devised a way to cause different amount of acidification with the same amount of proton influx by manipulating the intracellular pH buffering capacity. Intracellular pH is considered to be buffered by HCO_3^- and depriving extracellular HCO_3^- would likely cause efflux of intracellular HCO_3^- and result in low buffering capacity of the intracellular pH (Fig. 14; Zhang et al., 2010). Consistent with this idea, acidification measured by SNARF-5F imaging was significantly stronger in extracellular 5 mM HEPES buffer solution compared with extracellular $NaHCO_3$ buffer solution, even though both solutions were adjusted to the same pH (Fig. 14B). No significant difference was found in the amplitude of ChR2-induced BG depolarization upon switching from $NaHCO_3$-based to HEPES-based solution (Fig. 15A, upper panel); however, astrocytic ChR2-photoactivated PC-current was significantly increased (Fig. 15A, lower panel). The PC-current in HEPES was mostly blocked by GYKI (Fig. 15B), as in the normal $NaHCO_3$ solution (Fig. 5C). Glutamate sensitivity of PC-currents was not increased by switching the external solutions (Fig. 15C). These observations demonstrate that intracellular astrocytic acidification but not depolarization can be the direct trigger for glutamate release. The accurate calculation of the pH value from the experiments of SNARF-5F imaging is required to investigate the correlation between intracellular pH

and glutamate release.

4-3: Chapter 3: Acidification-triggered glutamate release from astrocytes accelerates brain damage upon ischemia

4-3-1. Ischemia induces glutamate release and acidosis

I turned to pathological situation where astrocyte-to-neuron signaling would likely operate maximally. Studying of such extreme situation may make complex system much simple. Upon brain ischemia, aerobic metabolism shuts down as a consequence of oxygen and glucose deprivation, lactate production from glycogen stored predominantly in astrocytes continues (Cataldo and Broadwell, 1986; Schurr et al., 1997), which leads to severe acidosis (Fig. 16A, B; Mutch and Hansen, 1984). Release of excess glutamate follows, which leads to neuronal cell death (Fig. 17A; Lau and Tymianski, 2010). However, the cellular source of glutamate and its release mechanism were unidentified. I focused on the astrocyte as they are the first responders to ischemic stress (Rossi et al., 2007) and hypothesized that strong acidification triggers excess glutamate release from astrocytes (Fig. 18).

Using acute cerebellar brain slices, ischemia was mimicked by oxygen and glucose deprivation (OGD) from continuously perfused artificial cerebrospinal fluid (ACSF) (Hamann et al., 2005). First, I verified that astrocytic acidification indeed occurs upon ischemic stress in acute cerebellar slices by using a pH-sensitive fluorescence dye, SNARF-5F AM (Fig. 16C). OGD elicited rapid reduction of SNARF-5F fluorescence ratio in BGs, indicating intracellular acidification. Cells other than BGs were also acidified and the time course of acidification was examined in granule cells (GCs) which have similar soma size as the BGs. Interestingly, the onset of the acidification was significantly faster in BGs than GCs (Fig. 16D).

Neuronal cell health was monitored by whole-cell patch clamp recordings from

Purkinje cells (PCs) (Fig. 17B). Shortly after the onset of OGD, transient burst firing occurred, which was followed by a plateau depolarization. These events could be considered as preludes to the eventual death of neurons. To monitor the excitatory drive evoked by OGD, PCs were recorded in voltage-clamp and picrotoxin (PIC) was applied to block inhibitory $GABA_A$ receptors. To exclude effects from neuronal transmitter release and focus on the astrocytic contribution to ischemic stress, tetrodotoxin (TTX) and Cd^{2+} were also applied. Within minutes, inward current developed, suggesting that OGD triggered release of excitatory substance from non-synaptic sources, presumably from glial cells (Fig. 17C). Whether this inward current is evoked by glutamate was examined with an AMPA receptor blocker alone (GYKI) or with a cocktail of glutamate receptor and transporter (GluR/T) blockers (NBQX, D-AP5, LY363785, and TBOA) (Fig. 17D). OGD-induced inward current was significantly blocked in both cases demonstrating that the majority of the inward current is due to glutamate. It should be noted, however, that some current remained suggesting that OGD also triggers effects other than glutamate release.

Results shown in chapter 2 suggests that astrocytic glutamate release can occur through 4,4'-diisothiocyanostilbene-2,2'-disulphonic acid (DIDS)-sensitive anion channels (Fig. 9A). Application of DIDS also partially inhibited the OGD-induced inward currents. These results suggest that release through DIDS-sensitive mechanisms could be one of the primary sources of excess glutamate release upon ischemia (Camacho et al., 2006; Liu et al., 2006; Seki et al., 1999), although DIDS-insensitive mechanisms also likely have a role.

4-3-2. Countering astrocytic acidosis inhibits neuronal damage

If astrocytic acidification were the key trigger of glutamate release upon ischemia, countering acidification with alkalization should be able to inhibit glutamate release and excitotoxicity. To selectively increase astrocytic intracellular pH, I generated a mouse line in which astrocyte population of glia, including BGs, specifically expresses ArchT, a light-sensitive outward proton pump (Han et al., 2011) by using the tTA-tetO system (Tsunematsu et al., 2013). Immunofluorescence and immunogold electron microscopic observations confirmed specific expression of ArchT in astrocyte (Fig. 19A, B). ArchT-photoactivation produced outward currents and hyperpolarization in BGs in voltage- and current-clamp modes, respectively (Fig. 19C). pH imaging also showed that ArchT-photoactivation reliably induced alkalization of BGs (Fig. 19D). Astrocytic ArchT-photoactivation dramatically inhibited OGD-induced inward currents in PCs (Fig. 20A). Astrocytic ArchT-photoactivation in control condition did not evoke any current in PCs and the effect was only evident in the OGD (Fig. 20B); thus, proton efflux from astrocyte or other ionic change does not directly produce any current in PCs. Furthermore, the blocking effect of astrocytic ArchT-photoactivation on OGD-induced PC-currents was nearly equal to that of GluR/T blockers application (Fig. 20A, middle) and was occluded in the presence of GluR/T blockade (Fig. 20A, right). ArchT effect was also observed at near-physiological temperature (Fig. 21A).

As DIDS could only block half of the OGD-induced current (Fig. 17D) and as the ArchT effect was only partially occluded by DIDS (Fig. 21B), there likely exists DIDS-sensitive and -insensitive astrocytic glutamate release mechanisms, both of which are pH sensitive. As glutamate uptake by glutamate transporters is voltage dependent (Bergles et al., 1997), it is possible that glutamate release is not suppressed but the uptake is facilitated in astrocyte which is hyperpolarized by ArchT-photoactivation. To

examine this possibility, OGD was induced in the presence of TBOA. Astrocytic ArchT-photoactivation blocked OGD-induced PC-currents similarly even in the presence of TBOA (Fig. 21C). Taken together, these data suggest that astrocytic pH change is an upstream causal factor of glutamate release upon ischemia (Fig. 22).

I next examined whether intermittent astrocytic ArchT-photoactivation could prevent deterioration of the healthiness of neurons upon ischemia. Excitatory current recorded from PCs in voltage-clamp increased upon OGD and over 1 nA of inward current was observed within 20 min. I next introduced intermittent astrocytic ArchT-photoactivation after detecting inward currents of more than 300 pA. Further development of inward current was prominently suppressed (Fig. 23A). The inward current could not be suppressed completely, suggesting the presence of additional unidentified mechanisms that lead to the increased conductance. Similarly, in current-clamp recordings from PCs in the absence of pharmacological agents, astrocytic ArchT-photoactivation was introduced after burst firing emerged upon OGD (Fig. 23B). Without the photoactivation, PCs soon reached plateau depolarization whereas photoactivation suppressed this indication of cell deterioration.

Could simply countering acidosis with astrocytic alkalization exert a neuroprotective action upon ischemia? To answer this question, ischemia in the cerebellum *in vivo* was created by using a photosensitive dye, rose bengal (Watson et al., 1985). Rose bengal was injected intra-arterially and focal ischemic region was created by exciting this dye via an optic fiber placed above the cerebellum and thrombosis was artificially created. Three hours after creation of thrombosis, severe neuronal degeneration was confirmed (Fig. 24A). To quantify the level of damage, brain sections were scored based on the relative loss of PCs and the degenerated area (Fig. 24B). In

one group of mice, astrocytic ArchT-photoactivation was intermittently applied from 0.5 to 2.5 hours after the creation of thrombosis. In this group, progressive generation of infarct area was significantly inhibited at 3 hours from photothrombosis (Fig. 24C, D). These results demonstrate that countering of astrocyte acidosis can reduce brain damage upon ischemia.

4-3-3. OGD response is different in the thalamus

All of the above studies were done in the cerebellum. Because of the morphological apposition of BG processes to neuronal elements, astrocyte-to-neuron signaling is most easily detected in the cerebellum. I next assessed whether the same principle governing astrocyte-to-neuron signaling would operate in other brain regions. I focused on the thalamus as this region is known to be prone to ischemic damage. I prepared thalamic slices obtained from mice expressing ChR2 or ArchT in astrocytes (Fig. 25A). Thalamic neuron in ventral posterolateral thalamus showed relatively small current response to astrocytic ChR2 photostimulation (Fig. 25B). This current was partly inhibited by AMPAR blocker, GYKI, indicating that glutamate is released in response to ChR2 photostimulation as in the cerebellum. In the cerebellar PCs, only AMPARs are expressed with no expression of NMDARs. In contrast, neuron in the thalamus expresses NMDARs as well. The remaining current in GYKI could be mediated by NMDARs, which could be assessed by NMDAR blocker such as D-AP5. This was not done yet. Astrocytic ArchT photostimulation dramatically reduced OGD induced inward current in thalamic neuron (74.3%; Fig. 25C). However, the blocking effect of glutamate receptor blockers (NBQX, 10 μM and D-AP5, 150 μM) on OGD current was only partial (41.7%). Although I have only one data so far, this result suggests that

OGD stress in the thalamus produces not only glutamate release but also other factors that generate neuronal excitatory response. However, it is also possible that the remaining component is the glutamate release through the glutamate transporter. Astrocytic ArchT photostimulation-effect on thalamic neuron was only slightly reduced in the presence of glutamate receptor blockers (ratio, 0.90; n = 1). ArchT photostimulation likely inhibits astrocytic glutamate release in the thalamus as well; however, interestingly, ArchT photostimulation was much efficient in inhibiting excitatory drive which is not mediated by glutamate. These results indicate that astrocytic ArchT photostimulation effects differ among brain regions. Astrocytic glutamate release inhibition by ArchT photostimulation was clearly demonstrated in the cerebellum. Thalamic studies revealed another component that emerges upon ischemia, which is not mediated by glutamate but is still strongly inhibited by ArchT photostimulation. The identity of this component remains to be solved.

5. Discussion

Here, I showed that astrocyte-photostimulation drives neuronal activity, synaptic plasticity, and behavior alternations. One of the signaling pathways is astrocytic glutamate release (Chapter 1). The mechanism of astrocyte-photostimulated glutamate release was found to be triggered by intracellular acidification (Chapter 2). To focus on the pH-dependent astrocyte-to-neuronal activity, I turned to pathological condition where this signaling would likely manifest most. I found that astrocytic acidosis causes excess release of glutamate, which becomes the major cause of ischemic brain damage (Chapter 3).

5-1. Signaling pathway from astrocyte to neuron

There is increasing evidence that astrocytes send signals to neurons. Several reports suggest that astrocytes modulate synaptic activity by releasing ATP, adenosine, glutamate, and D-serine (Fellin et al., 2004; Halassa and Haydon, 2010; Kakegawa et al., 2011; Panatier et al., 2011). However, most of these experiments were performed in brain slice condition. Transgenic expression of ChR2 in astrocytes enables stimulation of a wide range of astrocytic population *in vivo*. Astrocyte-photostimulation *in vivo* induced *c-fos* elevation and behavior alternations (Fig. 3, 4). Slice patch clamp experiments showed that glutamate is one of the mediators for these astrocyte-photoacitivated neuronal responses (Fig. 5). However, astrocyte-photostimulation also causes changes in extracellular K^+, as K^+-channel-mediated currents in addition to ChR2-mediated currents were observed in BGs (Sasaki et al., 2012). Although my slice experiment data clearly demonstrates the existence of glutamate releasing pathway in astrocytes, it should be noted that *in vivo*

ChR2 photostimulation likely produces both glutamate and K^+. A recent report shows that excitatory input to astrocytes was disrupted by knocking out glutamate receptors specifically in astrocytes (Saab et al., 2012). In these mice, neuronal structure, synaptic plasticity, and motor learning were disturbed. In my study, astrocytic signal output was artificially controlled, which resulted in alternations of neuronal functions (Fig. 3, 4). These data suggest that bidirectional communication between astrocytes and neuron have an important role in the function of the brain.

5-2. Methods for evoking selective astrocyte-activation

To date, several techniques to activate astrocytes were attempted which includes application of agonist of group 1 mGluRs (Fellin et al., 2004), mechanical stimulation (Angulo et al., 2004), and direct depolarization (Jourdain et al., 2007). Uncaging of Ca^{2+} (Fellin et al., 2004; Perea and Araque, 2007) or utilizing transgenic mice expressing MRGA1 in astrocytes (Fiacco et al., 2007) were also tried. However, due to the lack of cell type specificity or the limited population of manipulating cells, most of them failed to be employed *in vivo* studies. Introducing transgenic mice line which expresses ChR2 selectively in astrocytes allowed us to manipulate astrocytic dynamics under *in vivo* awake conditions (Fig. 3, 4). However, it still remains unresolved whether our stimulation protocol was physiologically relevant, although astrocytic depolarization induced by photostimulation (2.7 ± 0.5 mV) was comparable to that induced by typical electrical stimulation (3.6 ± 0.5 mV) (Sasaki et al., 2012). Thus, further studies are required to reveal participation of astrocytes in neuronal circuit under more physiological conditions.

5-3. Mechanism of glutamate release from astrocytes

Astrocytic glutamate release has been suggested to be mediated by vesicular release (Jourdain et al., 2007) or by glutamate transporters (Szatkowski et al., 1990). Recently, there is increasing evidence that glutamate release occurs through anion channels (Liu et al., 2006; Woo et al., 2012). Astrocyte-photostimulated glutamate release is also mediated through anion channels which are DIDS-sensitive but NPPB-insensitive (Fig. 9A, D). Trigger for these anion channels opening is proton influx (Fig. 13-15) and calcium is not involved in this process (Fig. 10). I was surprised of these results because many of reports suggest that astrocytic glutamate release is calcium-dependent (Fellin et al., 2004; Halassa and Haydon, 2010), although functional significance of astrocytic Ca^{2+} has also been questioned (Agulhon et al., 2010; Sun et al., 2013). I was not able to determine the molecular identity of the anion channels which release glutamate in response to a proton dynamics. However, there are reports indicating the presence of pH-dependent anion channels (Cavelier and Attwell, 2005; Lambert and Oberwinkler, 2005; Zifarelli et al., 2008) and pH-dependent amino acid transporters (Sakai et al., 2003; Weiss et al., 2005). In addition, pH-dependent astrocytic ATP release in the brain stem has been shown (Gourine et al., 2010). These reports support our findings which suggest that proton-sensitive and channel-mediated gliotransmitter release occurs in astrocytes. Thus, pH could be a key astrocytic intracellular signal, which is as pivotal as Ca^{2+}, although the role of pH may differ among different brain regions (Fig. 25, Kasymov et al., 2013).

5-4. pH dependent astrocytic glutamate release upon cerebellar ischemia

In chapter 3, I showed that astrocytic acidosis upon ischemia causes excess

glutamate release which deteriorates neuronal healthiness. Countering of astrocytic acidification with ArchT dramatically inhibited glutamate release and the following cell death. However, it should be noted that I am not proposing that H^+-triggered astrocytic glutamate release is the only mechanism underlying liberation of excess glutamate upon ischemia. Most of the current experiments were done in TTX and Cd^{2+} to focus on the glial component but neurons have also been shown to release glutamate during the initial stage of ischemia by vesicular release and reversal of neuronal and astrocytic glutamate transporters has also been shown to occur (Gebhardt et al., 2002; Hamann et al., 2005; Rossi et al., 2007). The relative role of each component is difficult to assess as blocking one component will also disrupt the interplay between all components. However, our data do show that suppression of astrocytic glutamate release alone by astrocytic ArchT-photoactivation can sustain hyperpolarization of neurons in half of the cells in slices in the absence of all pharmacological agents for some time (Fig. 23B) and save the brain from large structural damage *in vivo* (Fig. 24C, D). Therefore, controlling astrocytic pH may be an effective therapeutic strategy for intervention of ischemic brain damage. Conceivable therapeutic strategy involve simple delivering of cell-permeable strong pH buffer or pharmacological agents directed to facilitate H^+ extrusion from astrocytes. It is also important to identify which channel or transporter is involved in the pH-dependent astrocytic glutamate release.

5-5. Difference of astrocytic function in the brain regions

In the thalamus, not only glutamate but also unknown factors produced neuronal excitatory current upon OGD stress (Fig. 25C). Interestingly, astrocytic ArchT photostimulation dramatically inhibited this excitatory current as well. These results

indicate that pH dependent signaling from astrocyte to neuron is mediated not only by glutamate release but also by unknown components in the thalamus.

5-6. Astrocytic pH

It is still not known whether pH-sensitive glutamate release occurs physiologically. However, it is known that astrocytic intracellular pH is transiently alkalized followed by a prolonged acidification in response to neuronal activity (Chesler and Kraig, 1989; Newman, 1996). It is also known that the ambient glutamate level in brain tissue is controlled by glutamate release from astrocytes (Cavelier and Attwell, 2005). Thus, astrocytic pH-change initiated by neuronal activity could adjust the level of the ambient glutamate, which could result in setting the tone of neuronal activity.

5-7. In the future

My study suggests that astrocytes are likely to have a powerful role in regulating neuronal activity and brain healthiness. It has been suggested that astrocytic activity is related to several brain diseases such as ischemia (Beppu et al., 2014), epilepsy (Wetherington et al., 2008), and neurodegenerative disease (Niranjan, 2014). In these situations, astrocytes exhibit abnormal activities such as excess gliotransmitter release, calcium increase, and cell volume change. Thus, further use of optogenetics to specifically manipulate astrocytic function is expected to unveil how astrocytes participate in genesis and progress of brain disease.

6. Acknowledgements

I would like to great thank Associate Prof. Ko Matsui for leading me to study science and also for his sound advices and mentorship. I would like to thank Dr. Takuya Sasaki for teaching me electrophysiological experiments and providing me helpful advices. I would like to thank Prof. Ryuichi Shigemoto for his critical advices and continuous encouragement. I also would like to thank Associate prof. Kenji F. Tanaka (Keio Univ.) and Prof. Akihiro Yamanaka (Nagoya Univ.) for providing me the transgenic animals. I also would like to thank Associate prof. Yugo Fukazawa (Nagoya Univ.) for providing me the immunostaining data and teaching me the immunohistochemical experiments. I would like to thank Dr. Tomomi Tsunematsu for cheering up me during my research life. I also would like to thank all my laboratory members in Division of Cerebral Structure in NIPS and Division of Interdisciplinary Medical Science in Tohoku Univ. for their advice and encouragements.

7. References

Agulhon, C., Fiacco, T.A., and McCarthy, K.D. (2010). Hippocampal short- and long-term plasticity are not modulated by astrocyte Ca2+ signaling. Science *327*, 1250-1254.

Aiba, A., Kano, M., Chen, C., Stanton, M.E., Fox, G.D., Herrup, K., Zwingman, T.A., and Tonegawa, S. (1994). Deficient cerebellar long-term depression and impaired motor learning in mGluR1 mutant mice. Cell *79*, 377-388.

Allen, N.J., and Barres, B.A. (2009). Neuroscience: Glia - more than just brain glue. Nature *457*, 675-677.

Angulo, M.C., Kozlov, A.S., Charpak, S., and Audinat, E. (2004). Glutamate released from glial cells synchronizes neuronal activity in the hippocampus. J. Neurosci. *24*, 6920-6927.

Baude, A., Nusser, Z., Roberts, J.D., Mulvihill, E., McIlhinney, R.A., and Somogyi, P. (1993). The metabotropic glutamate receptor (mGluR1 alpha) is concentrated at perisynaptic membrane of neuronal subpopulations as detected by immunogold reaction. Neuron *11*, 771-787.

Beppu, K., Sasaki, T., Tanaka, K.F., Yamanaka, A., Fukazawa, Y., Shigemoto, R., and Matsui, K. (2014). Optogenetic countering of glial acidosis suppresses glial glutamate release and ischemic brain damage. Neuron *81*, 314-320.

Bergles, D.E., Dzubay, J.A., and Jahr, C.E. (1997). Glutamate transporter currents in bergmann glial cells follow the time course of extrasynaptic glutamate. Proc. Natl. Acad. Sci. U S A *94*, 14821-14825.

Berndt, A., Yizhar, O., Gunaydin, L.A., Hegemann, P., and Deisseroth, K. (2009). Bi-stable neural state switches. Nat. Neurosci. *12*, 229-234.

Camacho, A., Montiel, T., and Massieu, L. (2006). The anion channel blocker, 4,4'-dinitrostilbene-2,2'-disulfonic acid prevents neuronal death and excitatory amino acid release during glycolysis inhibition in the hippocampus in vivo. Neuroscience *142*, 1005-1017.

Cataldo, A.M., and Broadwell, R.D. (1986). Cytochemical identification of cerebral glycogen and glucose-6-phosphatase activity under normal and experimental conditions. II. Choroid plexus and ependymal epithelia, endothelia and pericytes. J. Neurocytol. *15*, 511-524.

Cavelier, P., and Attwell, D. (2005). Tonic release of glutamate by a DIDS-sensitive mechanism in

rat hippocampal slices. J. Physiol. *564*, 397-410.

Chesler, M., and Kraig, R.P. (1989). Intracellular pH transients of mammalian astrocytes. J. Neurosci. *9*, 2011-2019.

Fellin, T., Pascual, O., Gobbo, S., Pozzan, T., Haydon, P.G., and Carmignoto, G. (2004). Neuronal synchrony mediated by astrocytic glutamate through activation of extrasynaptic NMDA receptors. Neuron *43*, 729-743.

Fenno, L., Yizhar, O., and Deisseroth, K. (2011). The development and application of optogenetics. Annu. Rev. Neurosci. *34*, 389-412.

Fiacco, T.A., Agulhon, C., Taves, S.R., Petravicz, J., Casper, K.B., Dong, X., Chen, J., and McCarthy, K.D. (2007). Selective stimulation of astrocyte calcium in situ does not affect neuronal excitatory synaptic activity. Neuron *54*, 611-626.

Gebhardt, C., Korner, R., and Heinemann, U. (2002). Delayed anoxic depolarizations in hippocampal neurons of mice lacking the excitatory amino acid carrier 1. J. Cereb. Blood Flow Metab. *22*, 569-575.

Gourine, A.V., Kasymov, V., Marina, N., Tang, F., Figueiredo, M.F., Lane, S., Teschemacher, A.G., Spyer, K.M., Deisseroth, K., and Kasparov, S. (2010). Astrocytes control breathing through pH-dependent release of ATP. Science *329*, 571-575.

Halassa, M.M., and Haydon, P.G. (2010). Integrated brain circuits: astrocytic networks modulate neuronal activity and behavior. Annu. Rev. Physiol. *72*, 335-355.

Hamann, M., Rossi, D.J., Mohr, C., Andrade, A.L., and Attwell, D. (2005). The electrical response of cerebellar Purkinje neurons to simulated ischaemia. Brain *128*, 2408-2420.

Hamilton, N.B., and Attwell, D. (2010). Do astrocytes really exocytose neurotransmitters? Nat. Rev. Neurosci. *11*, 227-238.

Han, X., Chow, B.Y., Zhou, H., Klapoetke, N.C., Chuong, A., Rajimehr, R., Yang, A., Baratta, M.V., Winkle, J., Desimone, R.*, et al.* (2011). A high-light sensitivity optical neural silencer: development and application to optogenetic control of non-human primate cortex. Front. Syst. Neurosci. *5*, 18.

Hausser, M., and Roth, A. (1997). Dendritic and somatic glutamate receptor channels in rat cerebellar Purkinje cells. J. Physiol. *501 (Pt 1)*, 77-95.

Iino, M., Goto, K., Kakegawa, W., Okado, H., Sudo, M., Ishiuchi, S., Miwa, A., Takayasu, Y., Saito,

I., Tsuzuki, K.*, et al.* (2001). Glia-synapse interaction through Ca2+-permeable AMPA receptors in Bergmann glia. Science *292*, 926-929.

Ijichi, Y., Kiyohara, T., Hosoba, M., and Tsukahara, N. (1977). The cerebellar control of the pupillary light reflex in the cat. Brain Res. *128*, 69-79.

Jourdain, P., Bergersen, L.H., Bhaukaurally, K., Bezzi, P., Santello, M., Domercq, M., Matute, C., Tonello, F., Gundersen, V., and Volterra, A. (2007). Glutamate exocytosis from astrocytes controls synaptic strength. Nat. Neurosci. *10*, 331-339.

Kakegawa, W., Miyoshi, Y., Hamase, K., Matsuda, S., Matsuda, K., Kohda, K., Emi, K., Motohashi, J., Konno, R., Zaitsu, K.*, et al.* (2011). D-serine regulates cerebellar LTD and motor coordination through the delta2 glutamate receptor. Nat. Neurosci. *14*, 603-611.

Kasymov, V., Larina, O., Castaldo, C., Marina, N., Patrushev, M., Kasparov, S., and Gourine, A.V. (2013). Differential Sensitivity of Brainstem versus Cortical Astrocytes to Changes in pH Reveals Functional Regional Specialization of Astroglia. J. Neurosci. *33*, 435-441.

Katoh, A., Kitazawa, H., Itohara, S., and Nagao, S. (1998). Dynamic characteristics and adaptability of mouse vestibulo-ocular and optokinetic response eye movements and the role of the flocculo-olivary system revealed by chemical lesions. Proc. Natl. Acad. Sci. U S A *95*, 7705-7710.

Katz, B., and Miledi, R. (1966). Input-output relation of a single synapse. Nature *212*, 1242-1245.

Kleinlogel, S., Feldbauer, K., Dempski, R.E., Fotis, H., Wood, P.G., Bamann, C., and Bamberg, E. (2011). Ultra light-sensitive and fast neuronal activation with the Ca(2)+-permeable channelrhodopsin CatCh. Nat. Neurosci. *14*, 513-518.

Lambert, S., and Oberwinkler, J. (2005). Characterization of a proton-activated, outwardly rectifying anion channel. J. Physiol. *567*, 191-213.

Lau, A., and Tymianski, M. (2010). Glutamate receptors, neurotoxicity and neurodegeneration. Pflugers. Arch. *460*, 525-542.

Lee, S., Yoon, B.E., Berglund, K., Oh, S.J., Park, H., Shin, H.S., Augustine, G.J., and Lee, C.J. (2010). Channel-mediated tonic GABA release from glia. Science *330*, 790-796.

Li, D., Herault, K., Isacoff, E.Y., Oheim, M., and Ropert, N. (2012). Optogenetic activation of LiGluR-expressing astrocytes evokes anion channel-mediated glutamate release. J. Physiol. *590*, 855-873.

Liu, H.T., Tashmukhamedov, B.A., Inoue, H., Okada, Y., and Sabirov, R.Z. (2006). Roles of two types of anion channels in glutamate release from mouse astrocytes under ischemic or osmotic stress. Glia *54*, 343-357.

Liu, H.T., Akita, T., Shimizu, T., Sabirov, R.Z., and Okada, Y. (2009). Bradykinin-induced astrocyte-neuron signalling: glutamate release is mediated by ROS-activated volume-sensitive outwardly rectifying anion channels. J. Physiol. *587*, 2197-2209.

Lopez-Bendito, G., Shigemoto, R., Lujan, R., and Juiz, J.M. (2001). Developmental changes in the localisation of the mGluR1alpha subtype of metabotropic glutamate receptors in Purkinje cells. Neuroscience *105*, 413-429.

Ma, J., Matsumoto, M., Tanaka, K.F., Takebayashi, H., and Ikenaka, K. (2006). An animal model for late onset chronic demyelination disease caused by failed terminal differentiation of oligodendrocytes. Neuron Glia Biol. *2*, 81-91.

Matsui, K., and Jahr, C.E. (2003). Ectopic release of synaptic vesicles. Neuron *40*, 1173-1183.

Mutch, W.A., and Hansen, A.J. (1984). Extracellular pH changes during spreading depression and cerebral ischemia: mechanisms of brain pH regulation. J. Cereb. Blood Flow Metab. *4*, 17-27.

Nagel, G., Szellas, T., Huhn, W., Kateriya, S., Adeishvili, N., Berthold, P., Ollig, D., Hegemann, P., and Bamberg, E. (2003). Channelrhodopsin-2, a directly light-gated cation-selective membrane channel. Proc. Natl. Acad. Sci. U S A *100*, 13940-13945.

Newman, E.A. (1996). Acid efflux from retinal glial cells generated by sodium bicarbonate cotransport. J. Neurosci. *16*, 159-168.

Nimmerjahn, A., Mukamel, E.A., and Schnitzer, M.J. (2009). Motor behavior activates Bergmann glial networks. Neuron *62*, 400-412.

Niranjan, R. (2014). The role of inflammatory and oxidative stress mechanisms in the pathogenesis of Parkinson's disease: focus on astrocytes. Mol Neurobiol *49*, 28-38.

Panatier, A., Vallee, J., Haber, M., Murai, K.K., Lacaille, J.C., and Robitaille, R. (2011). Astrocytes are endogenous regulators of basal transmission at central synapses. Cell *146*, 785-798.

Perea, G., and Araque, A. (2007). Astrocytes potentiate transmitter release at single hippocampal synapses. Science *317*, 1083-1086.

Phillis, J.W., Ren, J., and O'Regan, M.H. (2000). Transporter reversal as a mechanism of

glutamate release from the ischemic rat cerebral cortex: studies with DL-threo-beta-benzyloxyaspartate. Brain Res. *868*, 105-112.

Piet, R., and Jahr, C.E. (2007). Glutamatergic and purinergic receptor-mediated calcium transients in Bergmann glial cells. J. Neurosci. *27*, 4027-4035.

Pizoli, C.E., Jinnah, H.A., Billingsley, M.L., and Hess, E.J. (2002). Abnormal cerebellar signaling induces dystonia in mice. J. Neurosci. *22*, 7825-7833.

Rossi, D.J., Brady, J.D., and Mohr, C. (2007). Astrocyte metabolism and signaling during brain ischemia. Nat. Neurosci. *10*, 1377-1386.

Saab, A.S., Neumeyer, A., Jahn, H.M., Cupido, A., Simek, A.A., Boele, H.J., Scheller, A., Le Meur, K., Gotz, M., Monyer, H*., et al.* (2012). Bergmann glial AMPA receptors are required for fine motor coordination. Science *337*, 749-753.

Sakai, K., Shimizu, H., Koike, T., Furuya, S., and Watanabe, M. (2003). Neutral amino acid transporter ASCT1 is preferentially expressed in L-Ser-synthetic/storing glial cells in the mouse brain with transient expression in developing capillaries. J. Neurosci. *23*, 550-560.

Sakatani, T., and Isa, T. (2004). PC-based high-speed video-oculography for measuring rapid eye movements in mice. Neurosci. Res. *49*, 123-131.

Sasaki, T., Beppu, K., Tanaka, K.F., Fukazawa, Y., Shigemoto, R., and Matsui, K. (2012). Application of an optogenetic byway for perturbing neuronal activity via glial photostimulation. Proc. Natl. Acad. Sci. U S A *109*, 20720-20725.

Schmitt, A., Gofferje, V., Weber, M., Meyer, J., Mossner, R., and Lesch, K.P. (2003). The brain-specific protein MLC1 implicated in megalencephalic leukoencephalopathy with subcortical cysts is expressed in glial cells in the murine brain. Glia *44*, 283-295.

Schonewille, M., Luo, C., Ruigrok, T.J., Voogd, J., Schmolesky, M.T., Rutteman, M., Hoebeek, F.E., De Jeu, M.T., and De Zeeuw, C.I. (2006). Zonal organization of the mouse flocculus: physiology, input, and output. J. Comp. Neurol. *497*, 670-682.

Schummers, J., Yu, H., and Sur, M. (2008). Tuned responses of astrocytes and their influence on hemodynamic signals in the visual cortex. Science *320*, 1638-1643.

Schurr, A., Payne, R.S., Miller, J.J., and Rigor, B.M. (1997). Glia are the main source of lactate utilized by neurons for recovery of function posthypoxia. Brain Res. *774*, 221-224.

Seki, Y., Feustel, P.J., Keller, R.W., Jr., Tranmer, B.I., and Kimelberg, H.K. (1999). Inhibition of

ischemia-induced glutamate release in rat striatum by dihydrokinate and an anion channel blocker. Stroke *30*, 433-440.

Sun, W., McConnell, E., Pare, J.F., Xu, Q., Chen, M., Peng, W., Lovatt, D., Han, X., Smith, Y., and Nedergaard, M. (2013). Glutamate-dependent neuroglial calcium signaling differs between young and adult brain. Science *339*, 197-200.

Szatkowski, M., Barbour, B., and Attwell, D. (1990). Non-vesicular release of glutamate from glial cells by reversed electrogenic glutamate uptake. Nature *348*, 443-446.

Tanaka, K.F., Ahmari, S.E., Leonardo, E.D., Richardson-Jones, J.W., Budreck, E.C., Scheiffele, P., Sugio, S., Inamura, N., Ikenaka, K., and Hen, R. (2010). Flexible Accelerated STOP Tetracycline Operator-knockin (FAST): a versatile and efficient new gene modulating system. Biol. Psychiatry *67*, 770-773.

Tanaka, K.F., Matsui, K., Sasaki, T., Sano, H., Sugio, S., Fan, K., Hen, R., Nakai, J., Yanagawa, Y., Hasuwa, H.*, et al.* (2012). Expanding the repertoire of optogenetically targeted cells with an enhanced gene expression system. Cell Rep. *2*, 397-406.

Tsunematsu, T., Tabuchi, S., Tanaka, K.F., Boyden, E.S., Tominaga, M., and Yamanaka, A. (2013). Long-lasting silencing of orexin/hypocretin neurons using archaerhodopsin induces slow-wave sleep in mice. Behav. Brain Res.

Watson, B.D., Dietrich, W.D., Busto, R., Wachtel, M.S., and Ginsberg, M.D. (1985). Induction of reproducible brain infarction by photochemically initiated thrombosis. Ann. Neurol. *17*, 497-504.

Weiss, M.D., Rossignol, C., Sumners, C., and Anderson, K.J. (2005). A pH-dependent increase in neuronal glutamate efflux in vitro: possible involvement of ASCT1. Brain Res. *1056*, 105-112.

Wetherington, J., Serrano, G., and Dingledine, R. (2008). Astrocytes in the epileptic brain. Neuron *58*, 168-178.

Woo, D.H., Han, K.S., Shim, J.W., Yoon, B.E., Kim, E., Bae, J.Y., Oh, S.J., Hwang, E.M., Marmorstein, A.D., Bae, Y.C.*, et al.* (2012). TREK-1 and Best1 channels mediate fast and slow glutamate release in astrocytes upon GPCR activation. Cell *151*, 25-40.

Yaguchi, T., and Nishizaki, T. (2010). Extracellular high K+ stimulates vesicular glutamate release from astrocytes by activating voltage-dependent calcium channels. J. Cell Physiol. *225*, 512-518.

Zhang, Z., Nguyen, K.T., Barrett, E.F., and David, G. (2010). Vesicular ATPase inserted into the plasma membrane of motor terminals by exocytosis alkalinizes cytosolic pH and facilitates endocytosis. Neuron *68*, 1097-1108.

Zifarelli, G., Murgia, A.R., Soliani, P., and Pusch, M. (2008). Intracellular proton regulation of ClC-0. J. Gen. Physiol. *132*, 185-198.

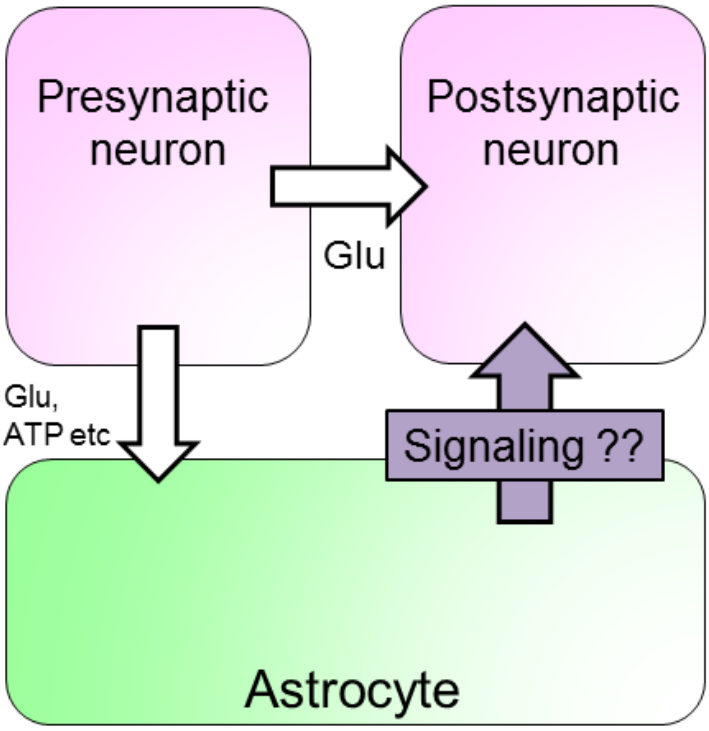

Figure 1. Schematics of the aim in this research

It is known that neuron send information not only to postsynaptic neurons but also to astrocytes. Recent studies suggest that astrocytes exhibits rapid and dynamic activity in response to neuronal activity. However, whether astrocytes can send information back to neurons was not demonstrated. If signaling pathway leading from astrocytes to neurons does not exist, the activity of astrocytes would have no role in our behavior and mind. Here, I aimed to seek the presence and significance of the interactive communication between astrocyte and neuron.

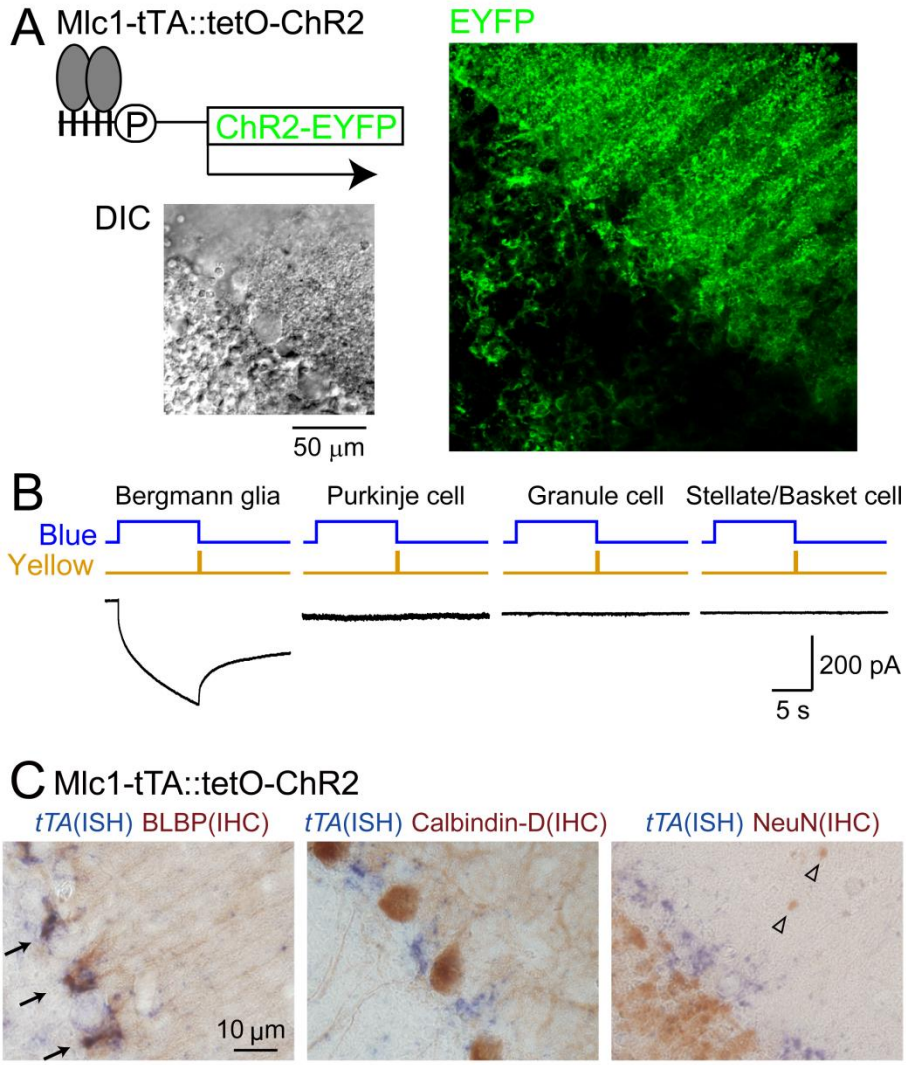

Figure 2. Generation of astrocyte-specific ChR2 expressing mice

(A) Crossing two lines of mice (Mlc1-tTA and tetO-ChR2(C128S)-EYFP) yielded mice in which ChR2(C128S)-EYFP was selectively expressed in Mlc1-positive astrocytes including cerebellar BGs. Bottom panels show a differential interference contrast (DIC) image and a confocal stack image of EYFP in an identical region of the parasagittal section of the cerebellum.

(B) Typical current traces in response to photostimulation recorded from a BG, PC, GC, and SC/BC (similar results from 24, 10, 10, and 11 cells, respectively). Recordings were

performed in the presence of TTX, Cd^{2+}, PIC, and NBQX to silence neuronal activity and extract ChR2 activity**.**

(C) Simultaneous *in situ* hybridization (ISH; blue) for *tTA* and immunohistochemistry (IHC; brown) for BLBP, calbindin-D, and NeuN. Images show *tTA* mRNA strongly colocalized with astrocyte specific marker, BLBP, but not with Purkinje cell marker, calbindin-D or neuronal marker, NeuN. Arrows in the left panel indicate *tTA* signals overlapping with BLBP-positive BGs and arrowheads in the right panel represent stellate/basket cells (SC/BCs) in the molecular layer devoid of *tTA* signals. Note that it is known that PCs are not labeled with NeuN (Mullen et al., 1992)

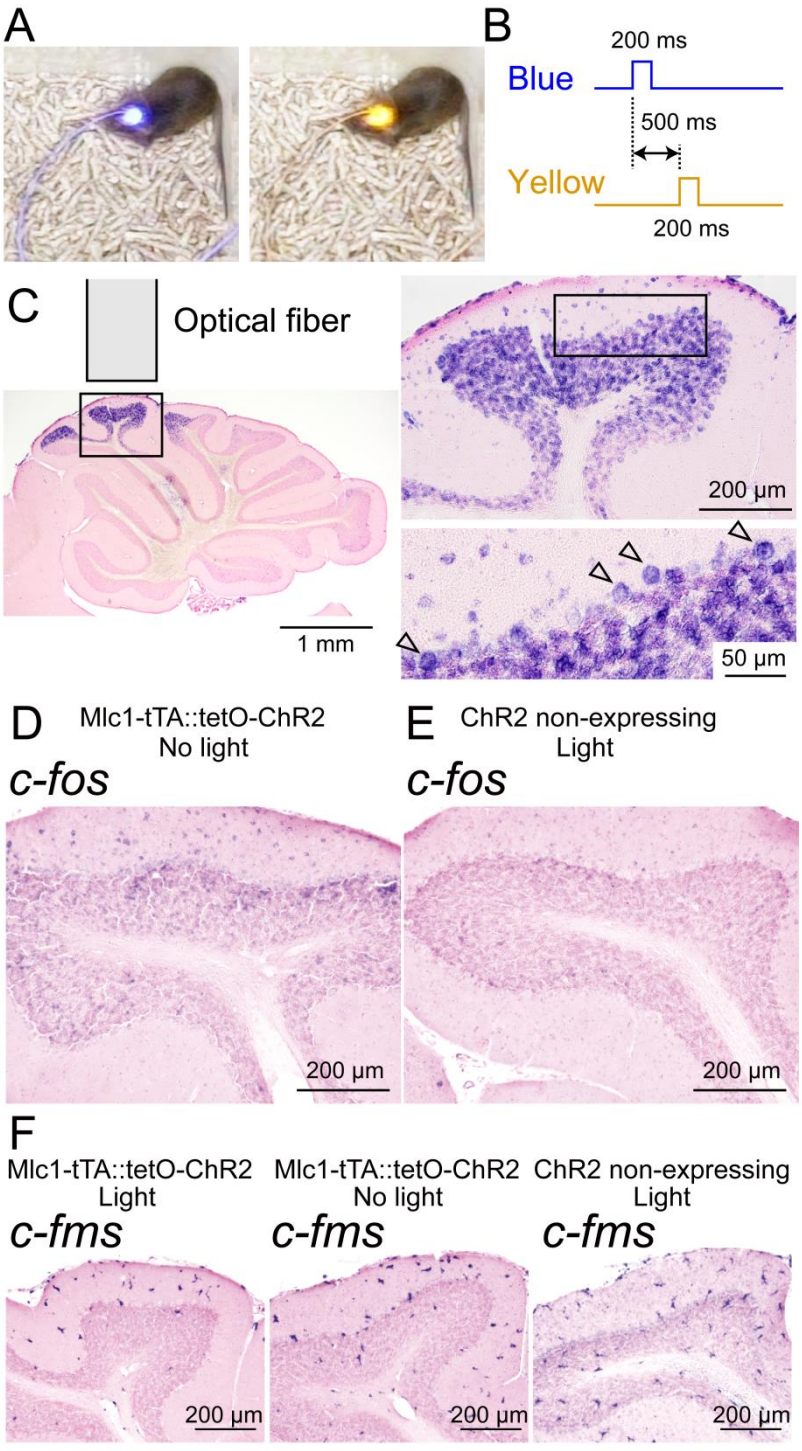
A
B
200 ms
Blue
500 ms
Yellow
200 ms
C
Optical fiber
1 mm
200 µm
50 µm
D
Mlc1-tTA::tetO-ChR2
No light
c-fos
200 µm
E
ChR2 non-expressing
Light
c-fos
200 µm
F
Mlc1-tTA::tetO-ChR2
Light
c-fms
200 µm
Mlc1-tTA::tetO-ChR2
No light
c-fms
200 µm
ChR2 non-expressing
Light
c-fms
200 µm

Figure 3. Astrocyte-photostimulation *in vivo* leads to neuronal activity

(A, B) Sequence of light applied *in vivo* via optical fiber placed on top of the cerebellar skull.

(C) *c-fos* mRNA (10 min after the photostimulation) was increased in PCs (arrowheads), GCs, and SC/BCs (n = 4 animals).

(D, E) Strong expression of *c-fos* mRNA was not detected in ChR2(+)-mice when no light was delivered through the placed optical fibers (D) or when the light was delivered to ChR2(C128S) non-expressing ChR2(−)-mice (E).

(F) *c-fms* mRNA expression, which gets increased in activated microglial cells, was not specifically increased surrounding the operated and illuminated area in mice with optical fiber placed on top of the skull. *c-fms* expression was similar in photostimulated and non-photostimulated Mlc1-tTA::tetO-ChR2-EYFP cerebellum as well as in photostimulated cerebellum from ChR2 non-expressing mice. This shows that the manipulations applied were not damaging to the brain tissue.

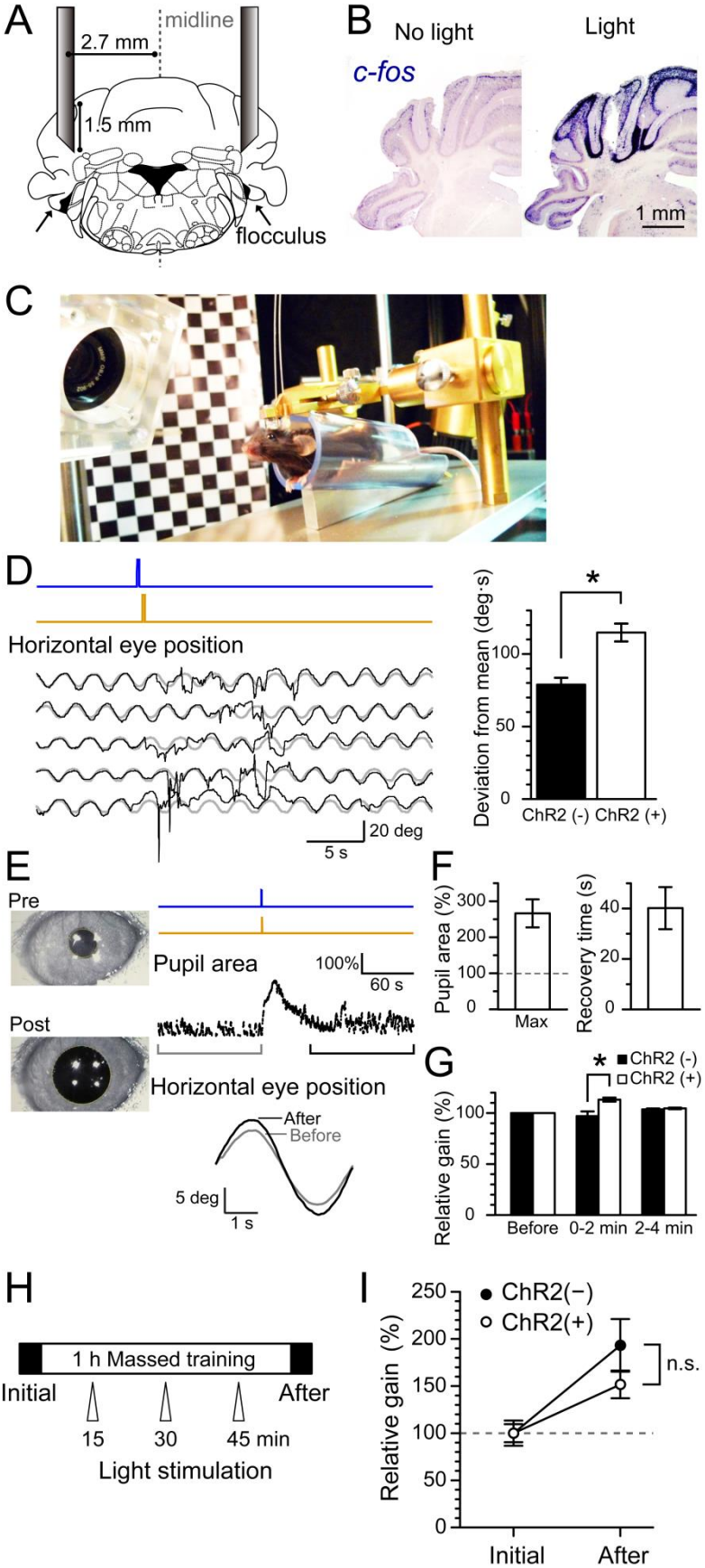
A
midline
2.7 mm
1.5 mm
flocculus
B
No light
Light
c-fos
1 mm
C
D
Horizontal eye position
20 deg
5 s
Deviation from mean (deg·s)
100
50
0
*
ChR2 (-) ChR2 (+)
E
Pre
Pupil area
100%
60 s
Post
Horizontal eye position
After
Before
5 deg
1 s
F
Pupil area (%)
300
200
100
0
Max
Recovery time (s)
40
20
0
G
* ChR2 (-)
ChR2 (+)
Relative gain (%)
100
50
0
Before
0-2 min
2-4 min
H
1 h Massed training
Initial
After
15
30
45 min
Light stimulation
I
ChR2(−)
ChR2(+)
Relative gain (%)
250
200
150
100
50
0
n.s.
Initial
After

Figure 4. Astrocyte-photostimulation changes behavior and learning

(A) Schematic of the optical fiber insertion location in the brain atlas (6.0 mm posterior to the bregma).

(B) Expression of *c-fos* mRNA was detected in the PC layer and ML/GL after a single incident of photostimulation (200 ms blue and 200 ms yellow light with an interval of 500 ms) delivered through the optical fibers.

(C) A photo of the HOKR experiment apparatus.

(D) HOKR was induced in head-fixed unanesthetized mice. The absolute difference was taken between the average horizontal eye movement (gray, 5 min prior to astrocyte-photostimulation) and the eye movement after astrocyte-photostimulation (black, same durations as above) via optic fibers inserted into the cerebellum and was integrated for 25 sec (n = 6 and 5 animals for ChR2(−) and ChR2(+), respectively; $*P < 0.01$, Student's t-test).

(E) Middle right, pupil area plotted against time. Lower right, 2 min average of the horizontal eye movement before the astrocyte-photostimulation (gray) and after the pupil area came back within 1 SD from the baseline (black).

(F) Peak increase in the pupil area and time for the cessation of pupil dilation were summarized (n = 5 animals). The time it took for the pupil to return within 1 SD from the baseline was defined as the recovery time.

(G) The average gain of horizontal eye movement at 0–2 min and 2–4 min after cessation of pupil dilation were normalized to the gain before the astrocyte-photostimulation for ChR2(+) mice. As pupil dilation did not occur in ChR2(−) mice, eye movements were measured after 0–2 min and 2–4 min after 45 sec

from photostimulation. Results were summarized for ChR2(−) and ChR2(+) (n = 6 and 5; *P < 0.05, Student's t-test).

(H) Checker pattern was presented with the horizontal and sinusoidal movement for 1 hour and photostimulation was delivered 3 times through the inserted optical fibers at the time indicated. HOKR gain was measured during the first 5 min (Initial) and the last 5 min (After) of the 1 hour session.

(I) The amount of HOKR gain increase was observed both in the ChR2 non-expressing mice (ChR2(−), n = 5 animals) and the ChR2 expressing mice (ChR2(+), n = 4 animals, P > 0.05).

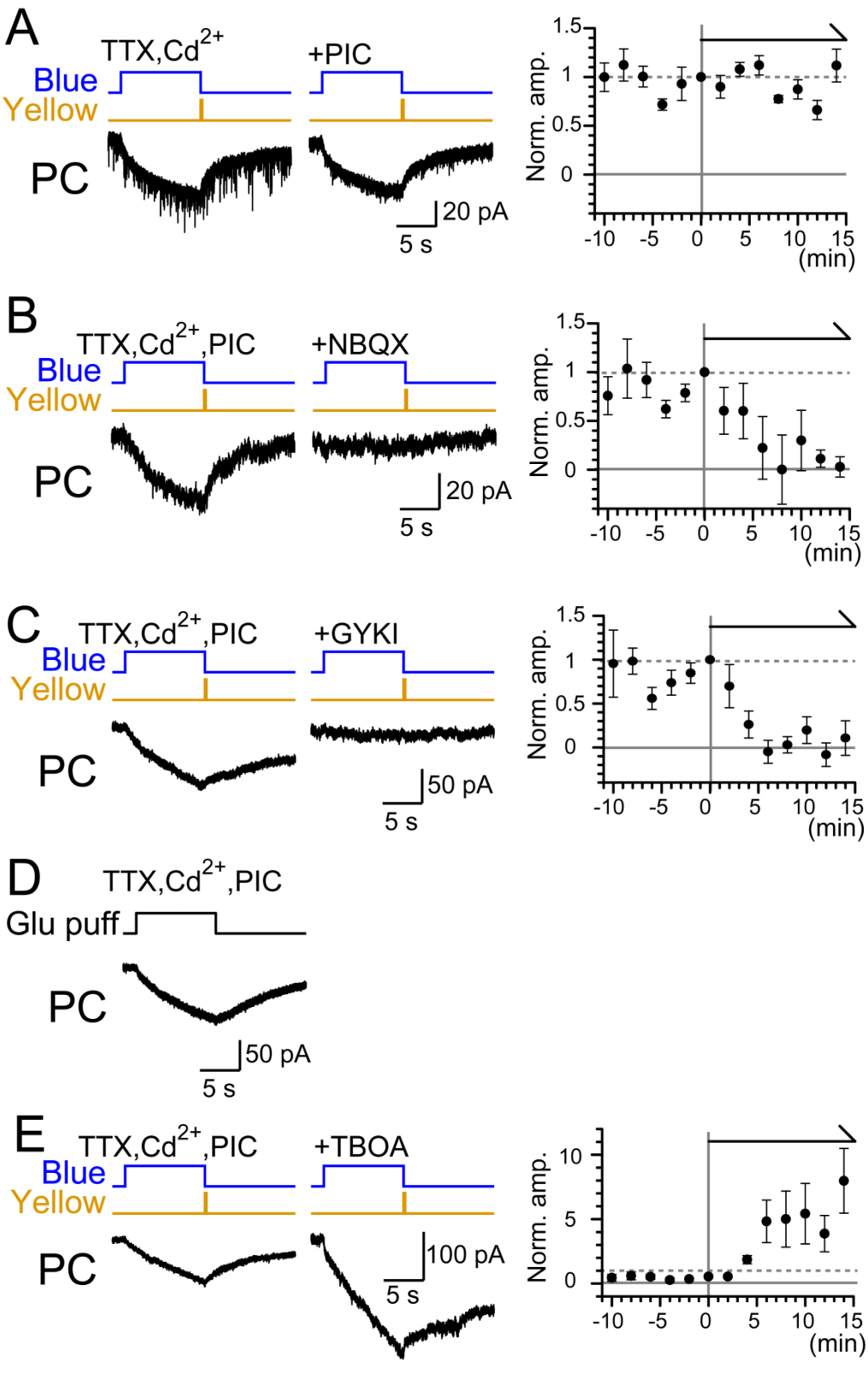
A
TTX,Cd2+
+PIC
Blue
Yellow
PC
20 pA
5 s
Norm. amp.
1.5
1
0.5
0
-10 -5 0 5 10 15
(min)
B
TTX,Cd2+,PIC
+NBQX
Blue
Yellow
PC
20 pA
5 s
Norm. amp.
1.5
1
0.5
0
-10 -5 0 5 10 15
(min)
C
TTX,Cd2+,PIC
+GYKI
Blue
Yellow
PC
50 pA
5 s
Norm. amp.
1.5
1
0.5
0
-10 -5 0 5 10 15
(min)
D
TTX,Cd2+,PIC
Glu puff
PC
50 pA
5 s
E
TTX,Cd2+,PIC
+TBOA
Blue
Yellow
PC
100 pA
5 s
Norm. amp.
10
5
0
-10 -5 0 5 10 15
(min)

Figure 5. Astrocyte-photostimulation triggers glutamate release

Astrocyte-photostimulated PC-currents (left) and time course of the amplitude change (right) before and after bath application of drugs (drug application from time = 0). Amplitudes of the current are plotted against time with the amplitude normalized to account for the rundown.

(A) Addition of PIC had no effect on the slow inward current, suggesting that GABA is not released in response to astrocyte-photostimulation (n = 5, $P > 0.05$). Notice that fast current noise does decrease with PIC application but this is likely due to the inhibition of $GABA_A$-mediated current in response to spontaneous quantal release of GABA from inhibitory SC/BCs.

(B, C) The PC-current was completely eliminated in the presence of an AMPAR blocker, NBQX (n = 4, $^*P < 0.05$, 0-2 min before versus 10–14 min after drug application, Paired t-test) and GYKI53655 (n = 5, $^{***}P < 0.001$).

(D) A current trace in a PC in response to puff application (10 s, 10 psi) of glutamate (100 μM). The kinetics of the current response was slow and similar to that observed for the astrocyte-photostimulated PC-current (similar results from 4 cells), which is consistent with the idea that the glutamate released from photostimulation diffuses through the tissue and produces the slow inward current in PCs.

(E) Inhibition of glutamate transporter by TBOA augmented the PC-current (n = 5).

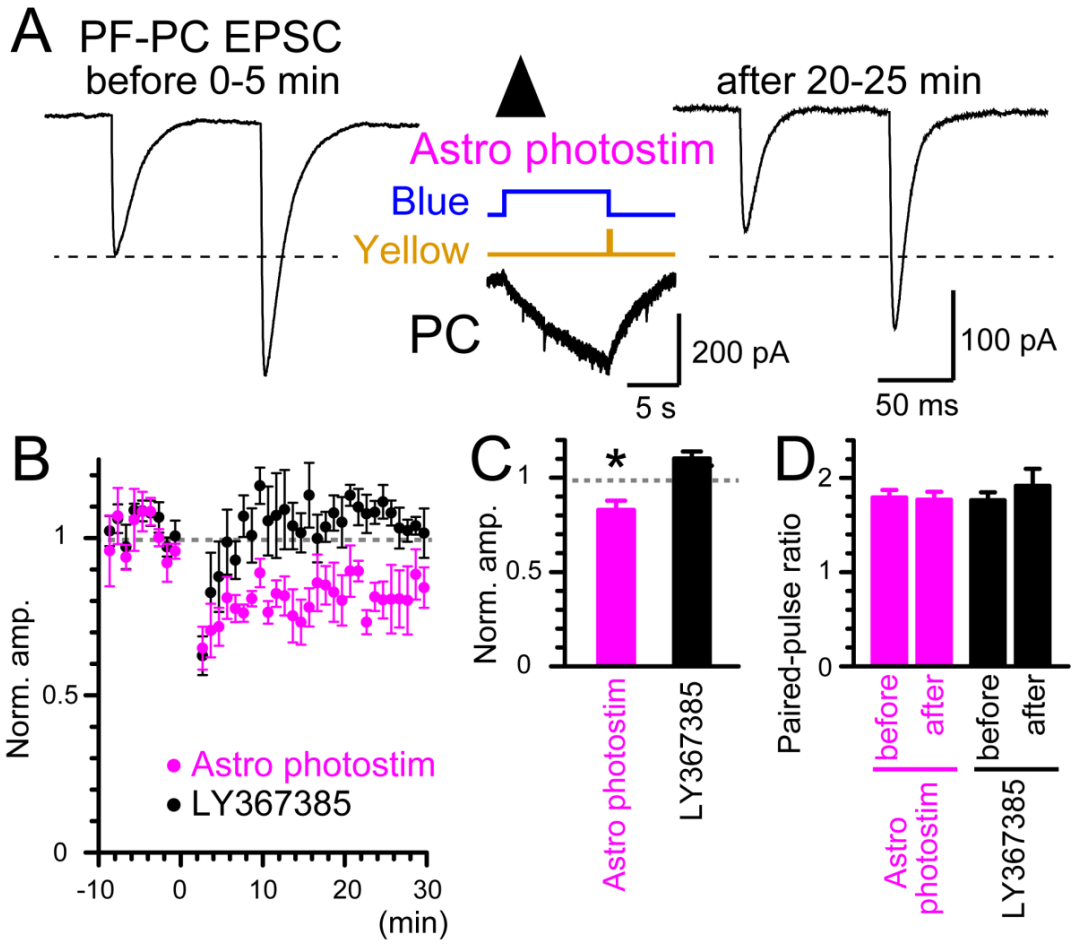
A
PF-PC EPSC
before 0-5 min
after 20-25 min
Astro photostim
Blue
Yellow
PC
200 pA
5 s
100 pA
50 ms
B
Norm. amp.
Astro photostim
LY367385
(min)
C1
Norm. amp.
Astro photostim
LY367385
D2
Paired-pulse ratio
before
after
Astro photostim
before
after
LY367385

Figure 6. Synaptic plasticity induced by asytocyte-photostimulation

(A) Electrically-stimulated PF-PC EPSCs in response to paired-pulse protocol (100-ms interval) before and after a single astrocyte-photostimulation. LTD of the PF-PC EPSC was observed.

(B) Time course of the first PF-PC EPSC amplitude (n = 5; LY367385, n = 5; *P < 0.05, Student's t-test). Photostimulation applied at time 0.

(C, D) Summary of the changes in the normalized EPSC amplitude (C) and the mean paired-pulse ratio (D) before and 20-25 min after the astrocyte-photostimulation. Application of an mGluR1 antagonist, 100 μM LY367385, blocked the LTD (P > 0.05, n = 5; Fig. 6C). No change in the input resistance of PCs was detected after photostimulation (Before 100.6 ± 10.5 MΩ; After 105.6 ± 8.9 MΩ; P > 0.05, paired t-test). The photostimulation did not significantly alter the EPSC paired-pulse ratio (P > 0.05, n = 5; Fig. 6D), implying that presynaptic components were not affected by the photostimulation.

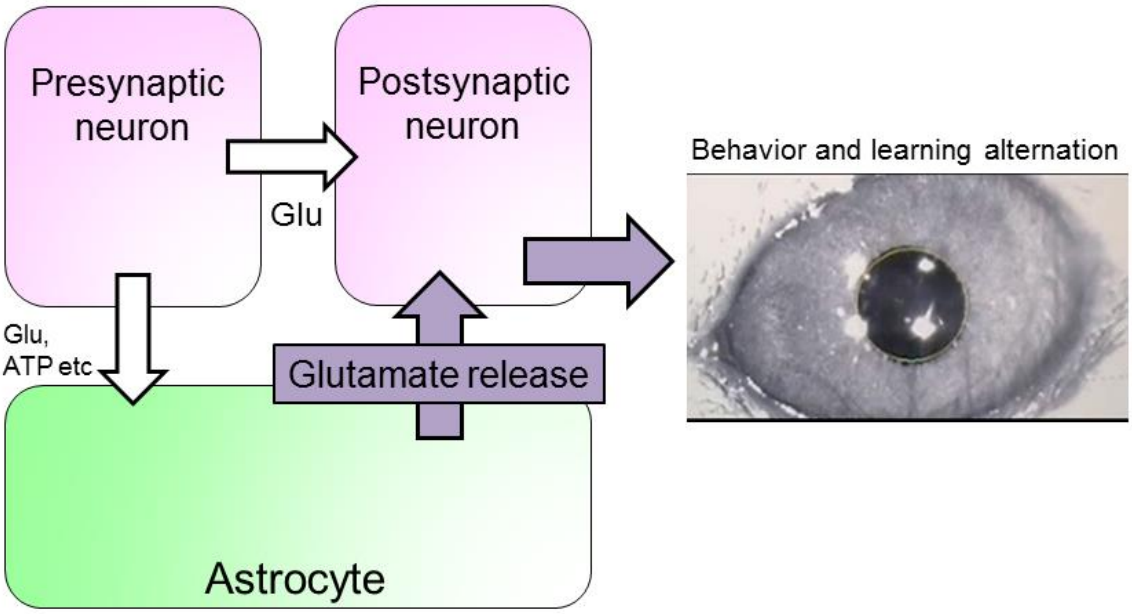

Figure 7. Short summary for chapter 1

In Chapter 1, I found that astrocytic glutamate release can induce neuronal activity. This signaling leads to behavior and learning changes by modulating synaptic plasticity. This result suggests a potential role of astrocytes in actively participating in the information processing in the brain.

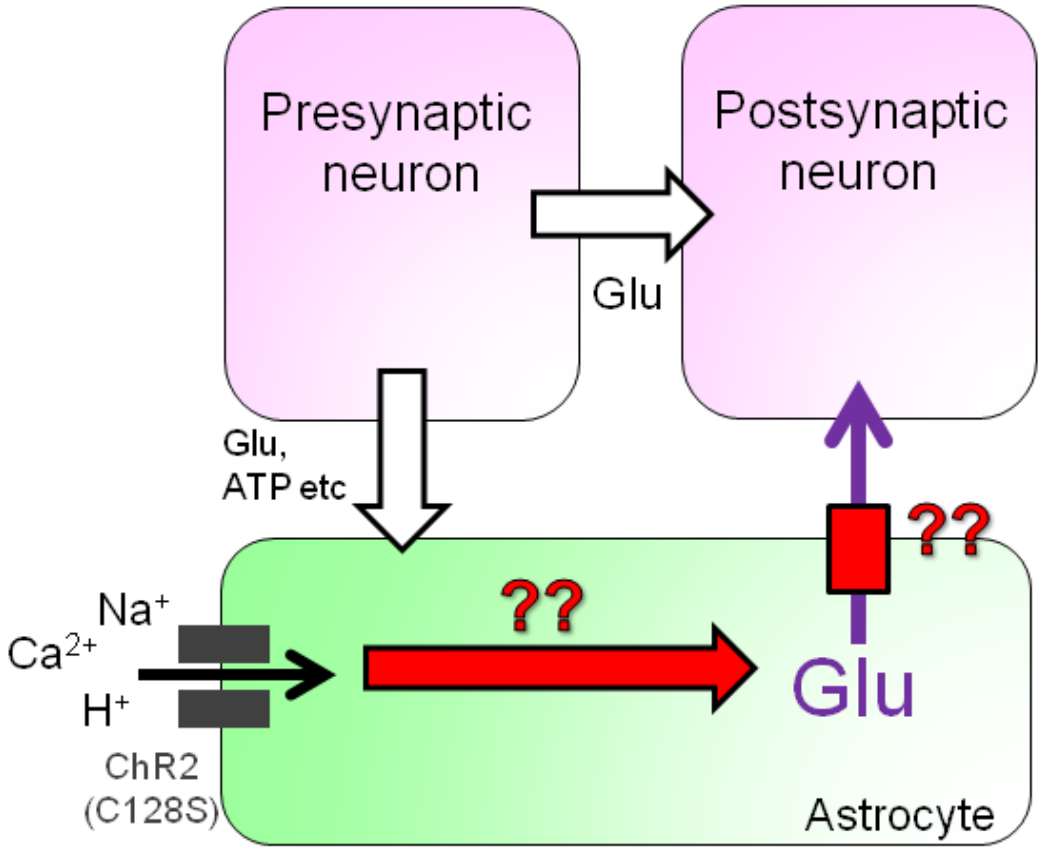

Figure 8. Identify the mechanism of glutamate release from astrocytes

In chapter 2, I investigated the mechanism of glutamate release from astrocytes induced by astrocyte-photostimulation.

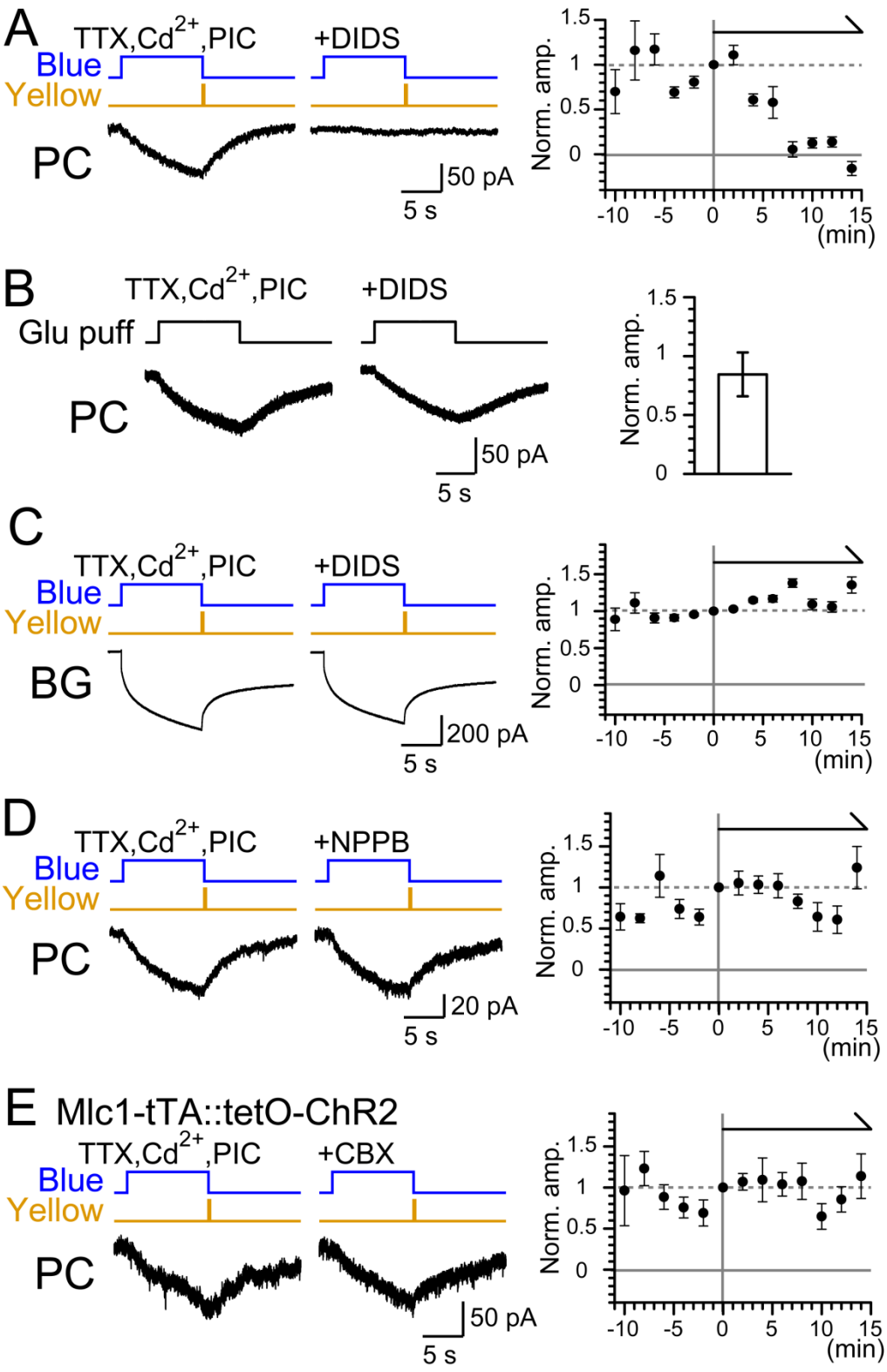
A
TTX,Cd2+,PIC
+DIDS
Blue
Yellow
PC
50 pA
5 s
Norm. amp.
1.5
1
0.5
0
-10
-5
0
5
10
15
(min)
B
TTX,Cd2+,PIC
+DIDS
Glu puff
PC
50 pA
5 s
Norm. amp.
1.5
1
0.5
0
C
TTX,Cd2+,PIC
+DIDS
Blue
Yellow
BG
200 pA
5 s
Norm. amp.
1.5
1
0.5
0
-10
-5
0
5
10
15
(min)
D
TTX,Cd2+,PIC
+NPPB
Blue
Yellow
PC
20 pA
5 s
Norm. amp.
1.5
1
0.5
0
-10
-5
0
5
10
15
(min)
E
Mlc1-tTA::tetO-ChR2
TTX,Cd2+,PIC
+CBX
Blue
Yellow
PC
50 pA
5 s
Norm. amp.
1.5
1
0.5
0
-10
-5
0
5
10
15
(min)

Figure 9. Glutamate release by astrocyte-photostimulation is mediated by the opening of DIDS-sensitive anion channels

(A) Inhibition of anion channels with DIDS abolished the PC-current (top, $n = 6$, ***$P < 0.001$)

(B) PC-currents in response to puff application (10 s, 10 psi) of glutamate (100 µM) were not significantly inhibited by DIDS treatment ($n = 7$, $P > 0.05$). This shows that inhibition of astrocyte-photostimulated PC-current by DIDS is not due to AMPAR inhibition by DIDS but due to inhibition of glutamate release by DIDS.

(C) BG photocurrent *per se* was not significantly altered by DIDS (bottom, n = 6, $P > 0.05$).

(D) Application of NPPB had no effect on the PC-currents ($n = 5$, $P > 0.05$).

(E) Blocking gap junctional hemichannels with CBX had no detectable effect on the amplitude of the astrocyte-photostimulated PC-currents (top, $n = 5$, $P > 0.05$, Student's t-test).

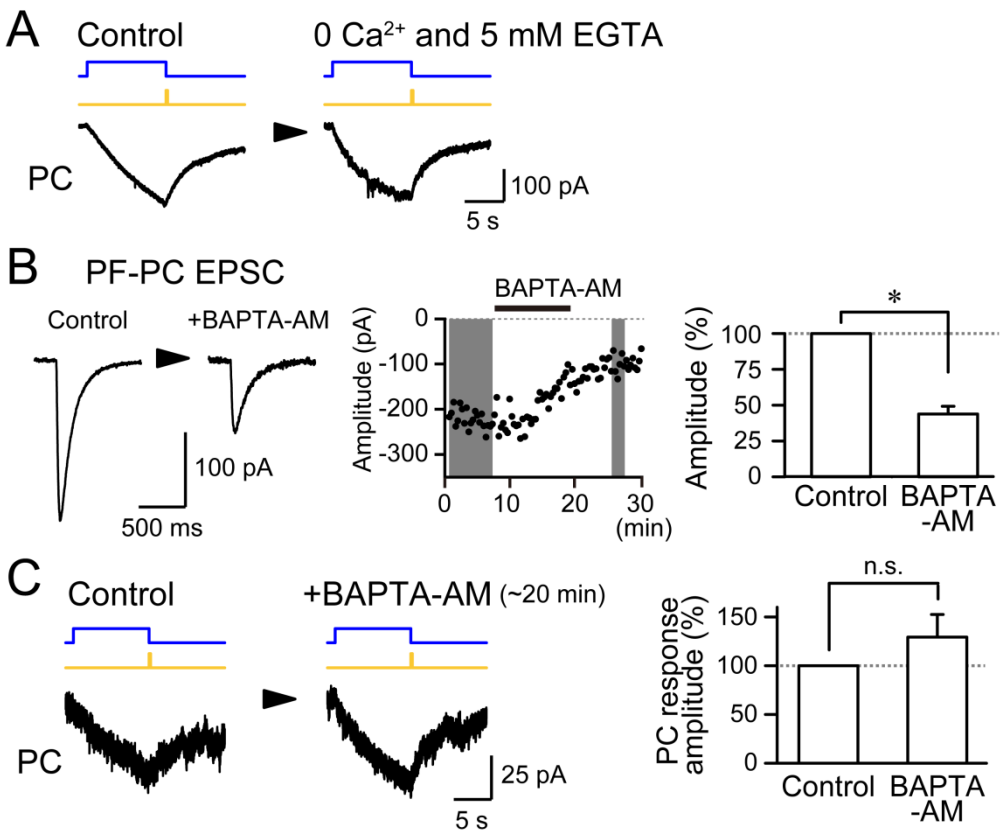

Figure 10. Calcium is not the trigger for astrocyte-photostimulated glutamate release

(A) Removing extracelular Ca^{2+} and adding EGTA (5 mM) did not inhibit astrocyte-photoactivated PC-currents. Similar recordings were made from two PCs.

(B) Parallel fiber (PF)-PC excitatory postsynaptic currents (EPSCs) were decreased after application of BAPTA-AM (100 μM) for 12 min (*P < 0.01, n = 4, Paired t-test). Left, sample traces before and after BAPTA-AM treatment. Middle, peak amplitudes of PF-PC EPSCs plotted against time. Right, summary of the BAPTA-AM effect. BAPTA-AM was sufficient in suppressing Ca^{2+}-dependent synaptic release.

(C) Astrocytic ChR2-photostimulated PC-currents remained intact under intracellular Ca^{2+} chelated condition with 100 μM BAPTA-AM. (P = 0.25, n = 8, Paired t-test).

These results (**A, C**) suggest that astrocytic glutamate release can occur with Ca^{2+} independent mechanisms. Error bars are s.e.m. Recordings in A, C were in TTX, Cd^{2+}, and PIC and recordings in B were in PIC only.

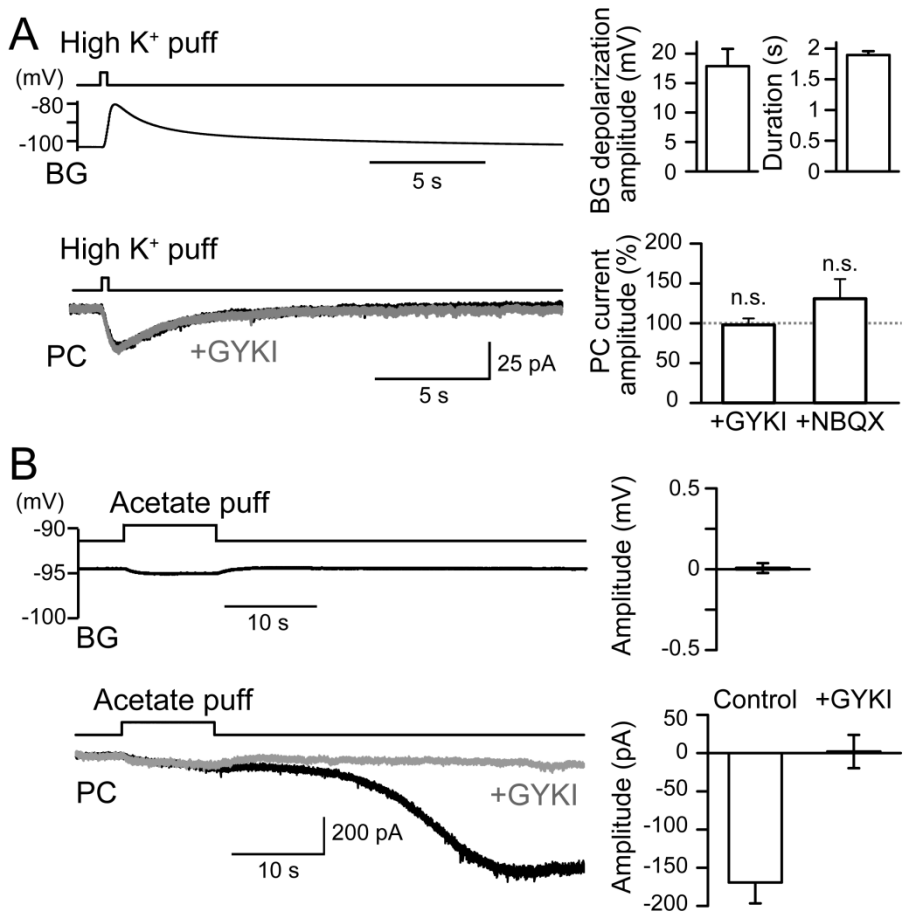

Figure 11. Acidification but not depolarization induces glutamate release from non-neuronal cells

(A) High K^+ (50 mM) solution was puff applied for 300 ms to evoke BG depolarization (upper trace). Duration of BG depolarization was measured as full-duration at half-maximum depolarization (right). Although these recordings were done in the presence of TTX, Cd^{2+}, and PIC, inward current under voltage-clamp mode was recorded in PCs in response to the high K^+ puff. This response is likely due to the influx of K^+ through leak K^+ conductance of PCs at resting potentials. This current was not affected by bath application of either GYKI or NBQX (lower gray trace) (P = 0.41, n = 3 for GYKI and P = 0.28, n = 5 for NBQX, Paired t-test). This result suggests that the depolarization induced by astrocytic ChR2-photoactivation itself is not the direct trigger

for glutamate release.

(B) As a method to raise intracellular H^+ concentration, acetate (20 mM) was puff applied (10 s). Acetate produced negligible hyperpolarization or depolarization in BGs (upper trace). Average amplitudes of the membrane potential change induced by the acetate puff (29.5-30 s after puff onset) were summarized (right, n = 5). Acetate did produce a slowly developing inward current in PCs (n = 4), which was not detected in the presence of GYKI, an AMPA receptor specific antagonist (n = 3, lower trace). Due to the quick rundown of the acetate effect, recordings from separate cells were compared. Average amplitudes of the current produced by the acetate puff (29.5–30 s after acetate puff onset) were summarized (right).

All recordings were in TTX, Cd^{2+}, and PIC. Error bars are s.e.m.

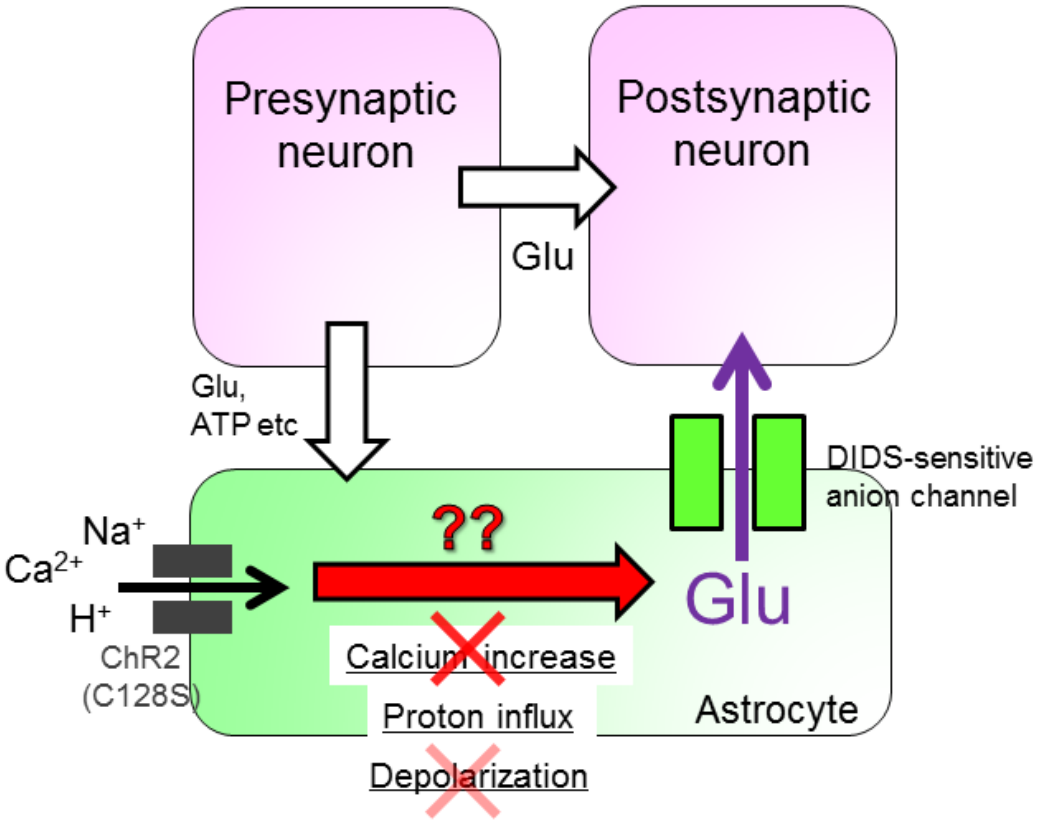

Figure 12. Identify a trigger for astrocyte-photostimulated glutamate release

Astrocytic ChR2-stimulation induces glutamate release through DIDS-sensitive channels. I aimed to find the direct trigger for the release. Astrocytic glutamate release by ChR2 stimulation occurs under calcium independent manner (Fig. 9). Also depolarization is not likely to be the trigger for the release as local appliacation of K^+ did not induce glutamate release from non-neuronal cells (Fig. 10B).

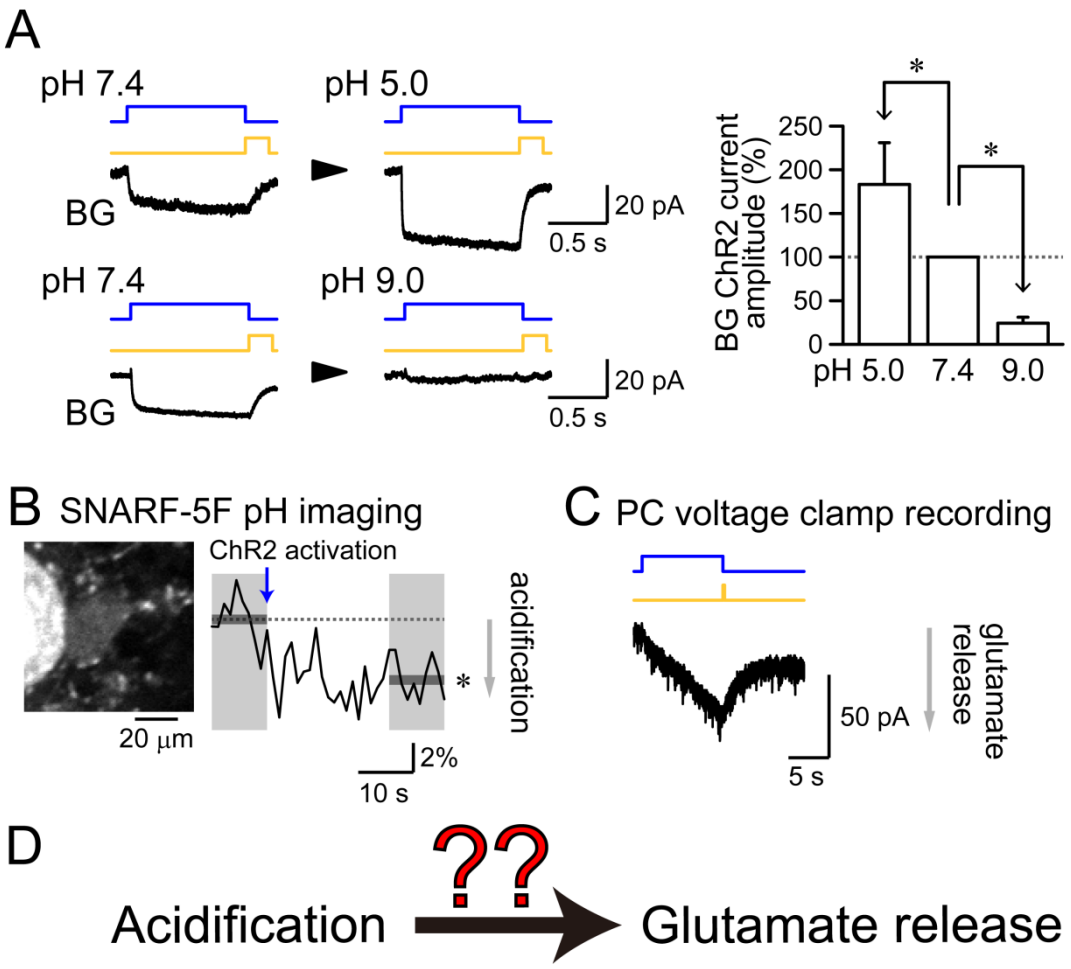

Figure 13. Astrocyte-photostimulation induces intracellular acidification and glutamate release

(A) H^+ permeability of ChR2(C128S) expressed on BGs was assessed by changing the extracellular pH from 7.4 to 5.0 (upper) or 9.0 (lower). Photocurrent amplitude at 100–200 ms from the blue light onset was significantly increased in pH 5.0 (**P* < 0.01, n = 5, Paired *t*-test), and decreased in pH 9.0 (**P* < 0.01, n = 8, Paired *t*-test).

(B) pH imaging of BGs with SNARF-5F. A single pulse of blue light opened the ChR2(C128S) channel for a prolonged time and intracellular acidification was induced.

(C) Astrocyte-photostimulation induces glutamate release which activates AMPAR on PCs (Fig. 5B, C).

(D) I hypothesized that ChR2-induced intracellular acidification is the direct trigger for the glutamate release.

Recordings in A-C were in TTX, Cd^{2+}, and PIC. Error bars are s.e.m.

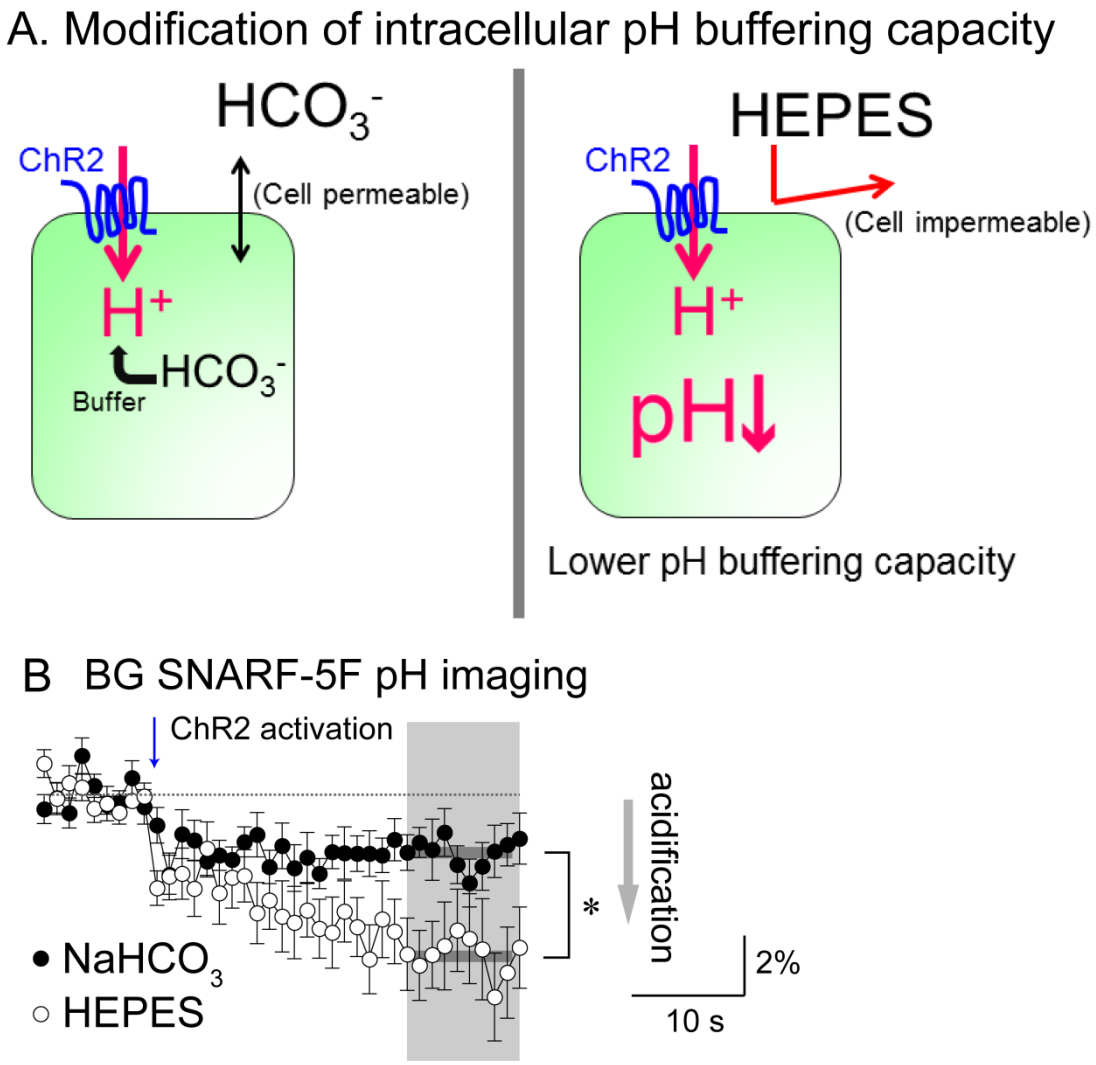

Figure 14. Method to modify intracellular pH buffering capacity

(A) Astrocyte-photostimulation induces both acidification and depolarization. To determine whether acidification is the direct trigger for glutamate release, I needed a method to isolate the acidification effect. Usually we use $NaHCO_3$ as an extracellular pH buffer in physiological slice experiments. Contrary to the $NaHCO_3$, another type of pH buffer, HEPES is not permeable through the cell membrane. Thus, if I use HEPES instead of $NaHCO_3$, intrinsic HCO_3^- would migrate to the extracellular space due to the concentration difference. As a result, intracellular pH buffering capacity would become lowered. I hypothesized that proton influx by ChR2 activation leads to more severe

acidification in HEPES than in $NaHCO_3$ due to the loss of pH buffering capacity, even though the depolarization evoked by the ChR2 activation are the same.

(**B**) pH imaging of BGs with SNARF-5F. A single pulse of blue light opened the ChR2(C128S) and intracellular acidification was induced. As expected, the acidification was stronger in HEPES compared to $NaHCO_3$ external buffer (*P < 0.01, n = 12 each, Student *t*-test).

Recordings in B were in TTX, Cd^{2+}, and PIC. Error bars are s.e.m.

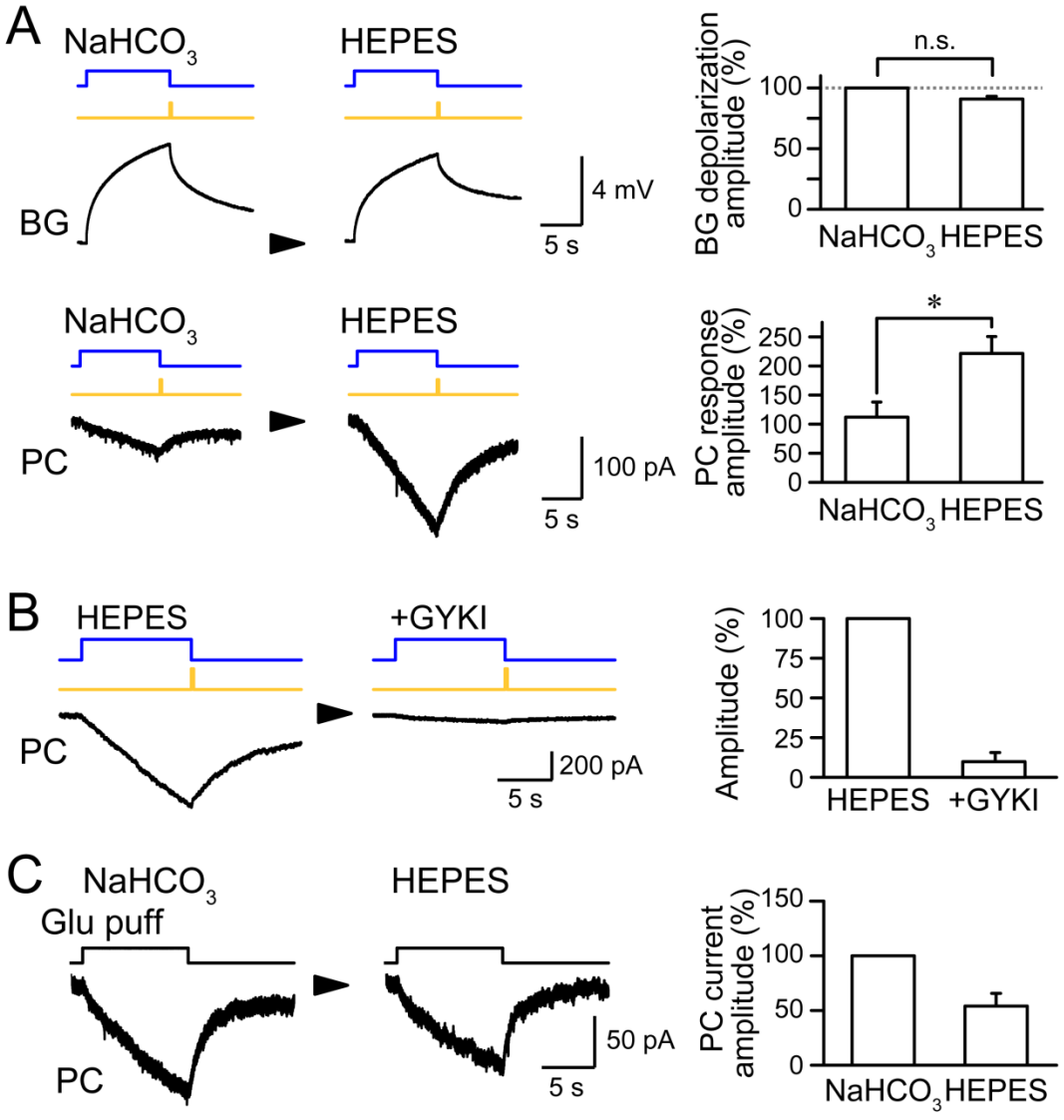

Figure 15. Stronger intracellular acidification leads to larger amount of glutamate release from astrocytes

(**A**) BG depolarization amplitude via ChR2(C128S) photoactivation was not affected by the external pH buffer (P = 0.07, n = 3, Paired t-test, upper panel), whereas astrocytic ChR2-photoactivated PC-currents became significantly larger by altering the buffer from $NaHCO_3$ to HEPES compared to $NaHCO_3$ to $NaHCO_3$ (*P < 0.05, n = 7 and 3, Student t-test).

(**B**) Application of GYKI, an AMPA receptor specific antagonist, blocked astrocytic ChR2-photoactivated PC-current in HEPES-based solution.

(**C**) Exchanging the extracellular solution from $NaHCO_3$-based to HEPES-based buffer did not increase PC-currents in response to glutamate (200 μM) puff application (n = 5) but rather decreased it. This result indicates that the increase in the astrocytic ChR2-photoactivated PC-current upon exchanging the extracellular solutions (Fig. 14A, bottom) was not due to the increase in the glutamate sensitivity of PC glutamate receptors.

All recordings were in TTX, Cd^{2+}, and PIC. Error bars are s.e.m.

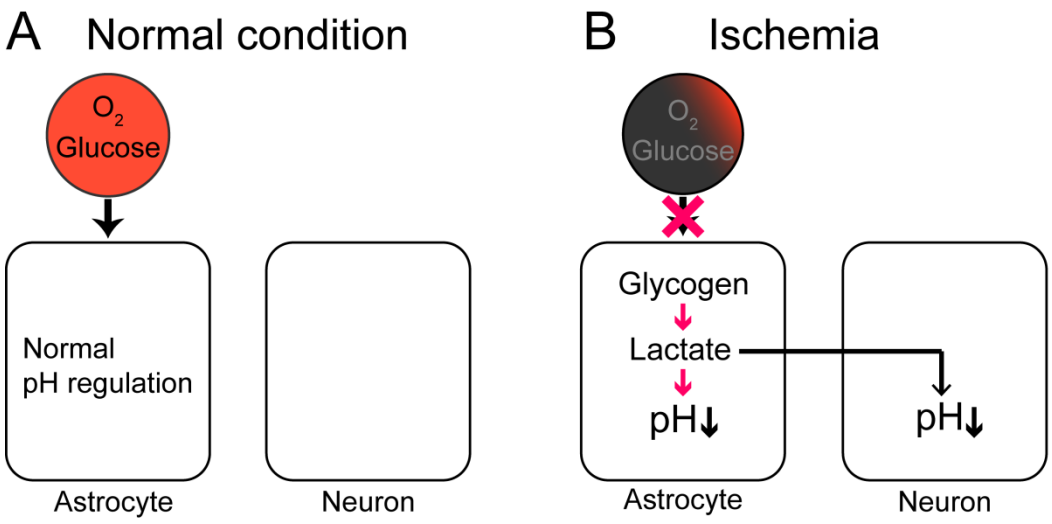
A
Normal condition
O2
Glucose
Normal
pH regulation
Astrocyte
Neuron
B
Ischemia
O2
Glucose
Glycogen
Lactate
pH↓
pH↓
Astrocyte
Neuron

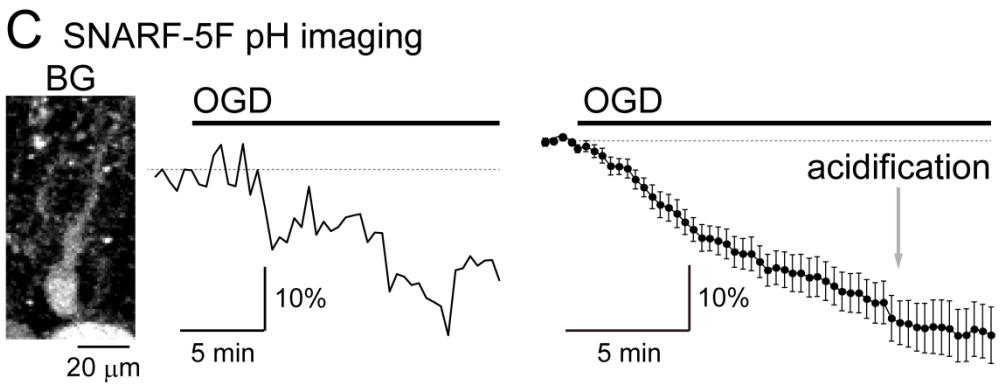
C
SNARF-5F pH imaging
BG
20 μm
OGD
10%
5 min
OGD
acidification
10%
5 min

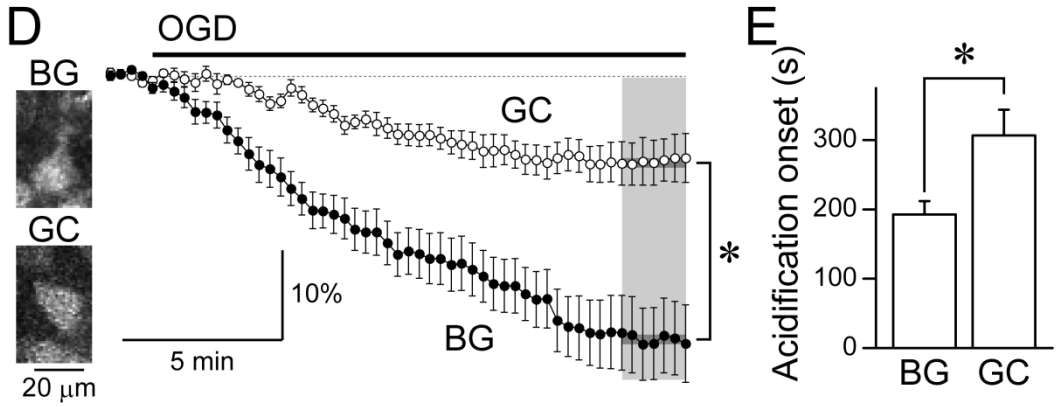
D
BG
GC
20 μm
OGD
GC
BG
10%
5 min
*
E
Acidification onset (s)
300
200
100
0
*
BG
GC

Figure 16. Ischemic stress produces astrocytic acidosis

In chapter 3, I studied the astrocytic contribution to excitotoxicity because pH mediated astrocyte-to-neuron signaling that I found would likely manifest under pathological conditions

(A, B) Schematics indicate the mechanism of astrocytic acidosis upon ischemic stress. When oxygen and glucose are supplied from blood vessels to brain cells, astrocytic pH is maintained at healthy levels (A). However, cessation of energy supply upon ischemia shuts down aerobic metabolism, whereas lactate production from glycogen stored predominantly in astrocyte continues, leading to its accumulation and to the rapid reduction of intracellular pH.

(C) A representative BG stained with SNARF-5F (left) and the change of fluorescence ratio ($R_{650/586}$) upon OGD, indicating intracellular acidification (middle). Average trace, right (n = 14).

(D) The average fluorescent ratios of BGs (filled circles) and GCs (opened circles) were plotted against time. 16-18 min after OGD onset, acidification level reached in BGs (29.2 ± 4.1%) was significantly higher compared with that in GCs (9.5 ± 2.4%) (**P* < 0.01, n = 12 each, Student *t*-test).

(E) Baseline noise of the fluorescence ratio during 0–100 s before OGD was calculated and the time it took for the acidification to cross the threshold of 2 SD of baseline was defined as the acidification onset. This was significantly faster in BGs (192.9 ± 19.1 s, n = 14) compared with GCs (306.7 ± 37.3 s, n = 12), **P* < 0.05, Student *t*-test. Upon OGD, lactate is produced predominantly in the astrocyte and this lactate is likely to be handed down to neurons via transporters, thus, producing this delay of neuronal acidification.

Recordings in C, D were TTX, Cd^{2+}, and PIC. Error bars are s.e.m.

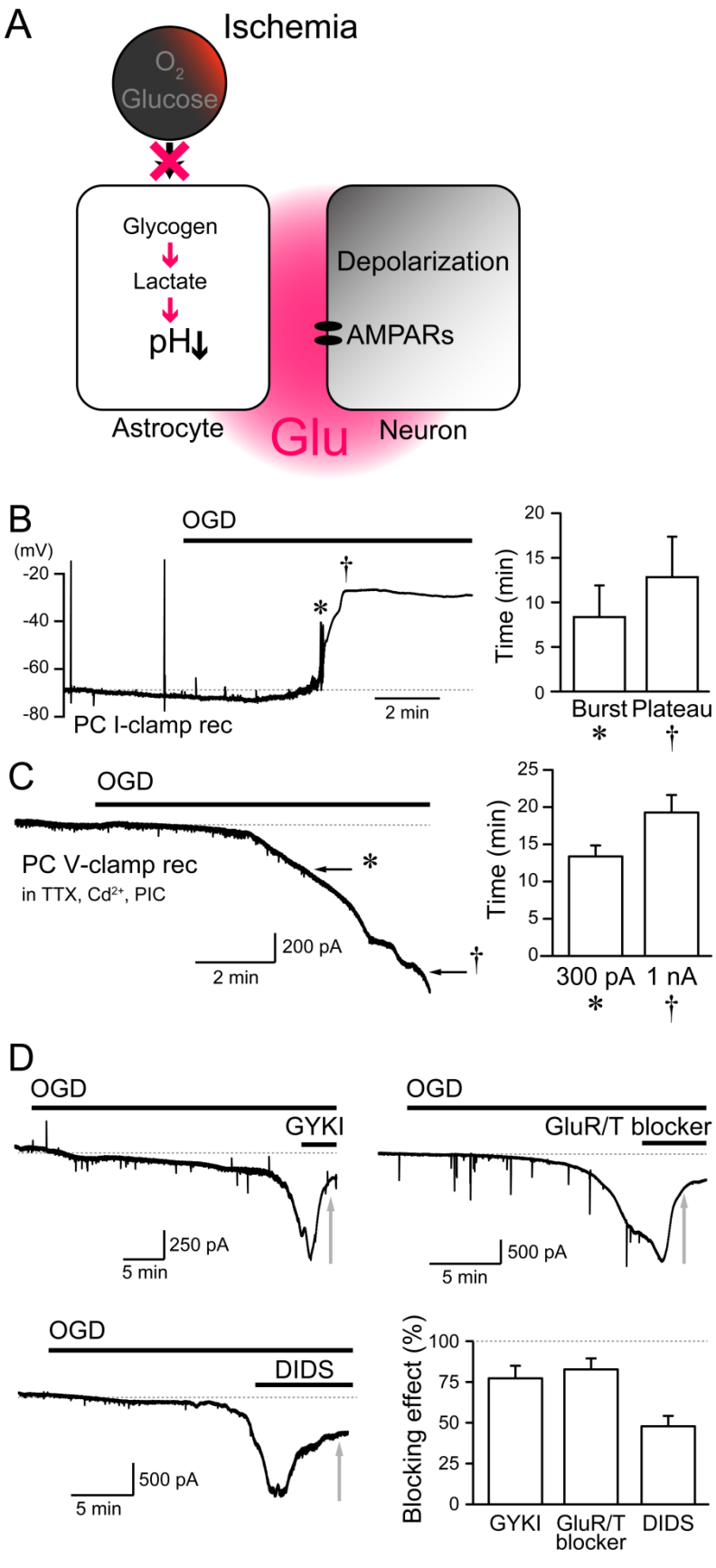
A
Ischemia
O2
Glucose
Glycogen
Lactate
pH
Depolarization
AMPARs
Astrocyte
Glu
Neuron
B
OGD
(mV)
-20
-40
-60
-80
PC I-clamp rec
2 min
Time (min)
Burst
Plateau
C
OGD
PC V-clamp rec
in TTX, Cd2+, PIC
200 pA
2 min
300 pA
1 nA
D
OGD
GYKI
250 pA
5 min
OGD
GluR/T blocker
500 pA
5 min
OGD
DIDS
500 pA
5 min
Blocking effect (%)
GYKI
GluR/T blocker
DIDS

Figure 17. Ischemic stress induces glutamate release from non-neuronal cells

(A) Upon ischemia, excess glutamate is released. However, cellular source of glutamate and its release mechanism upon ischemia remained unknown.

(B) Upon OGD, PCs displayed transient burst firing (*), followed by depolarization to a plateau (†). Average time of each event from the OGD onset is shown (right; Burst, n = 5; Plateau, n = 6).

(C) Excitatory current developed upon OGD in the presence of TTX, Cd^{2+}, and PIC. Average time to reach –300 pA (*, n = 22) and –1 nA (†, n = 14) is shown (right).

(D) An AMPA receptor blocker (all units in μM) (100 GYKI53655), glutamate receptor and transporter blockers (10 NBQX, 200 D-AP5, 100 LY363785, 50 TBOA), or an anion channel blocker (1,000 DIDS) suppressed OGD-induced PC-current (GYKI, $*P < 0.01$, n = 6; GluR/T blocker, $*P < 0.01$, n = 9; DIDS, $*P < 0.01$, n = 8). The DIDS effect was variable between cells (min = 22.8, max = 96.5%).

Recordings in C, D were in the presence of TTX, Cd^{2+}, and PIC. Error bars are s.e.m.

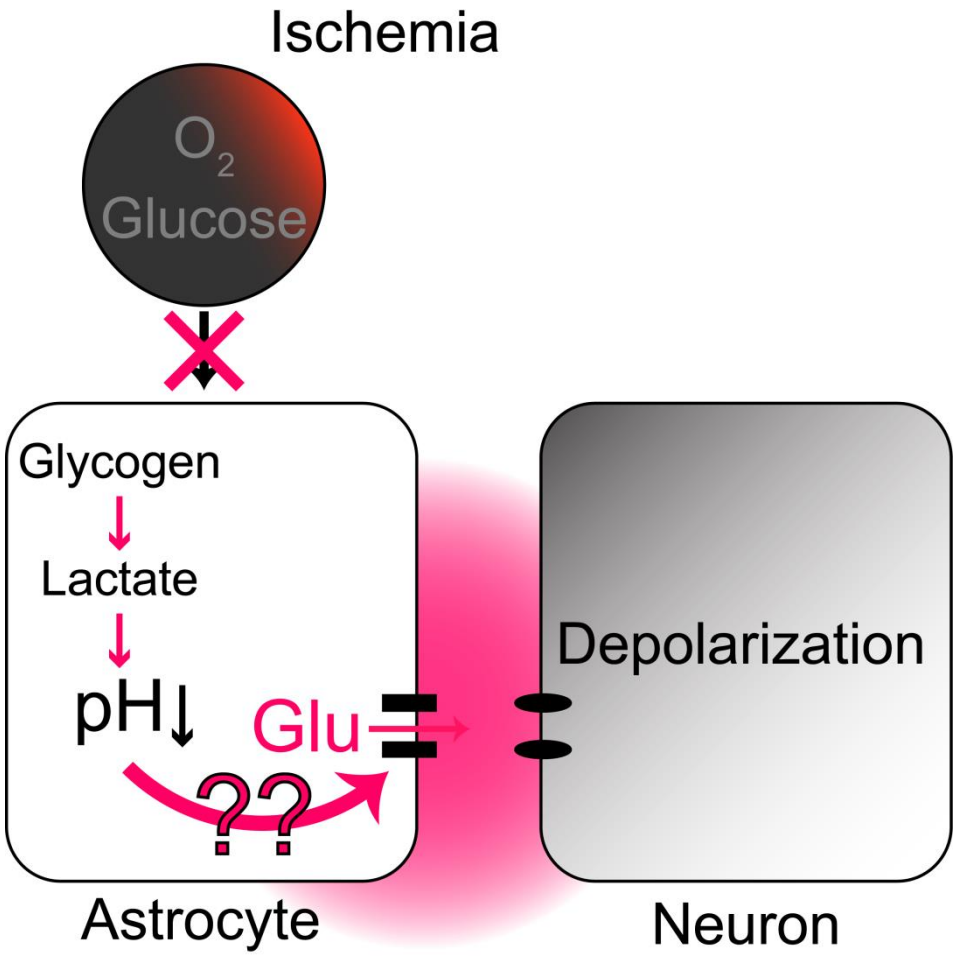

Figure 18. Two major events occur upon ischemia; acidosis and release of excess glutamate which leads to excitotoxicity. I hypothesized that there is a causal relationship between astrocytic acidosis and neuronal excitotoxicity.

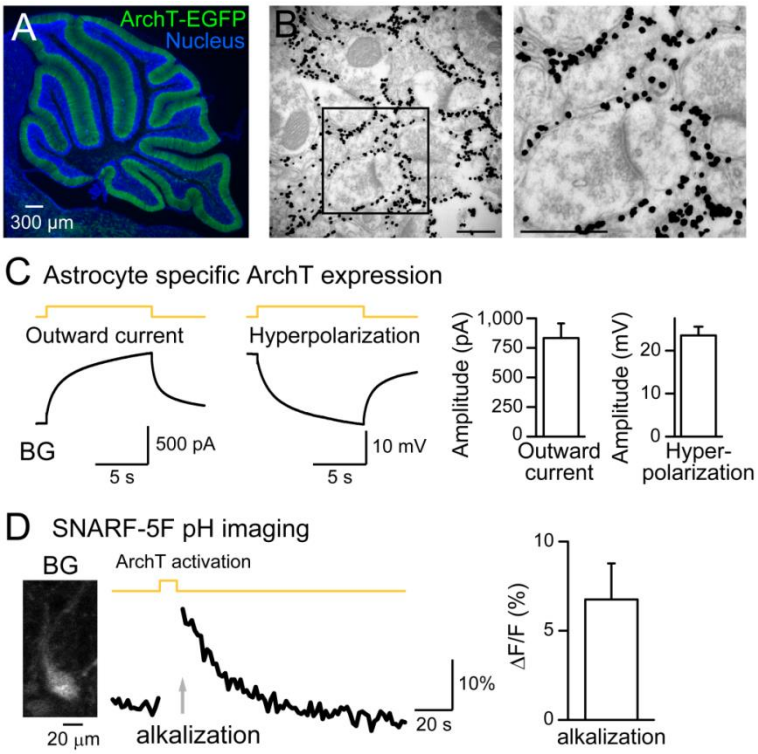

Figure 19. Generation of astrocyte specific ArchT expressing mice

(A) The bigenic mice, Mlc1-tTA::tetO-ArchT-EGFP, express ArchT selectively in astrocytes in cerebellar cortex. Blue, nuclear staining by H33342; Green, EGFP fluorescence.

(B) Immunogold EM of EGFP in the bigenic mice. EGFP was confirmed to be localized only in the astrocytes (288, 0, 0 and 1 immunogolds in identified astrocyte, presynaptic, postsynaptic and unidentifiable profiles, respectively). Scale bars indicate 500 nm in low (left) and high (right) magnified images.

(C) A typical current (left) and voltage (right) responses of BGs to ArchT-photoactivation (yellow). Right, average amplitudes of outward current (n = 9) and hyperpolarization (n = 6).

(D) pH imaging of a BG showed that alkalization was induced with astrocytic ArchT-photoactivation. Results summarized, right (n = 7).

Recordings in C, D were in TTX, Cd^{2+}, and PIC. Error bars are s.e.m.

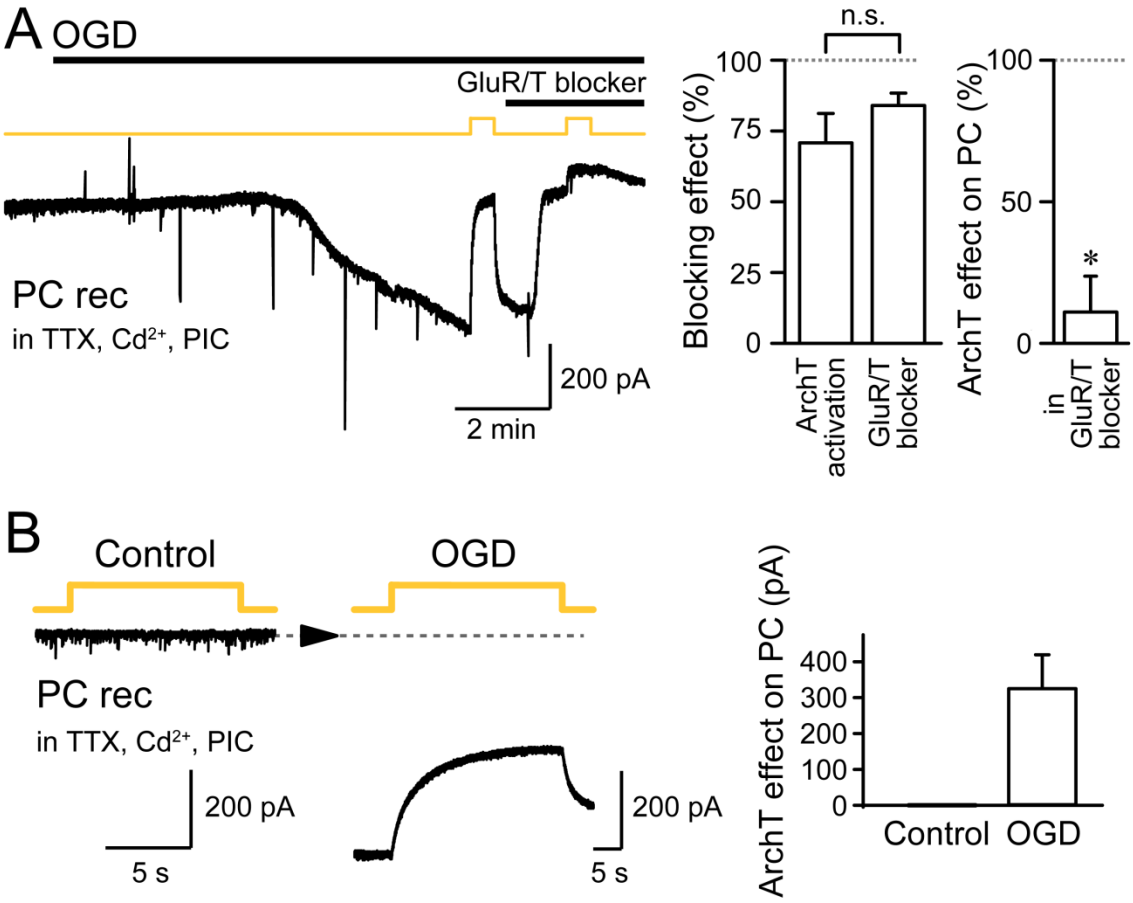

Figure 20. Astrocytic alkalization suppress OGD-induced PC-currents

(A) OGD-induced PC-currents were reduced by astrocytic ArchT-photoactivation (time constant to reach equilibrium = 1.6 ± 0.2 s, n = 8). The effect was not significantly different from the blocking effect of GluR/T blockers (P = 0.27, n = 8, 14, Student t-test). ArchT-photoactivation effect on PC was significantly reduced in the presence of GluR/T blockers (*P < 0.05, n = 5, Paired t-test).

(B) Astrocytic ArchT-photoactivated PC-currents were not detected under control condition, whereas the astrocytic ArchT-photoactivation generated outward PC currents during OGD. Average amplitudes of the outward current (9.5–10 s after yellow light application) were summarized (n = 7 each).

All recordings were in the presence of TTX, Cd^{2+}, and PIC. Error bars are s.e.m.

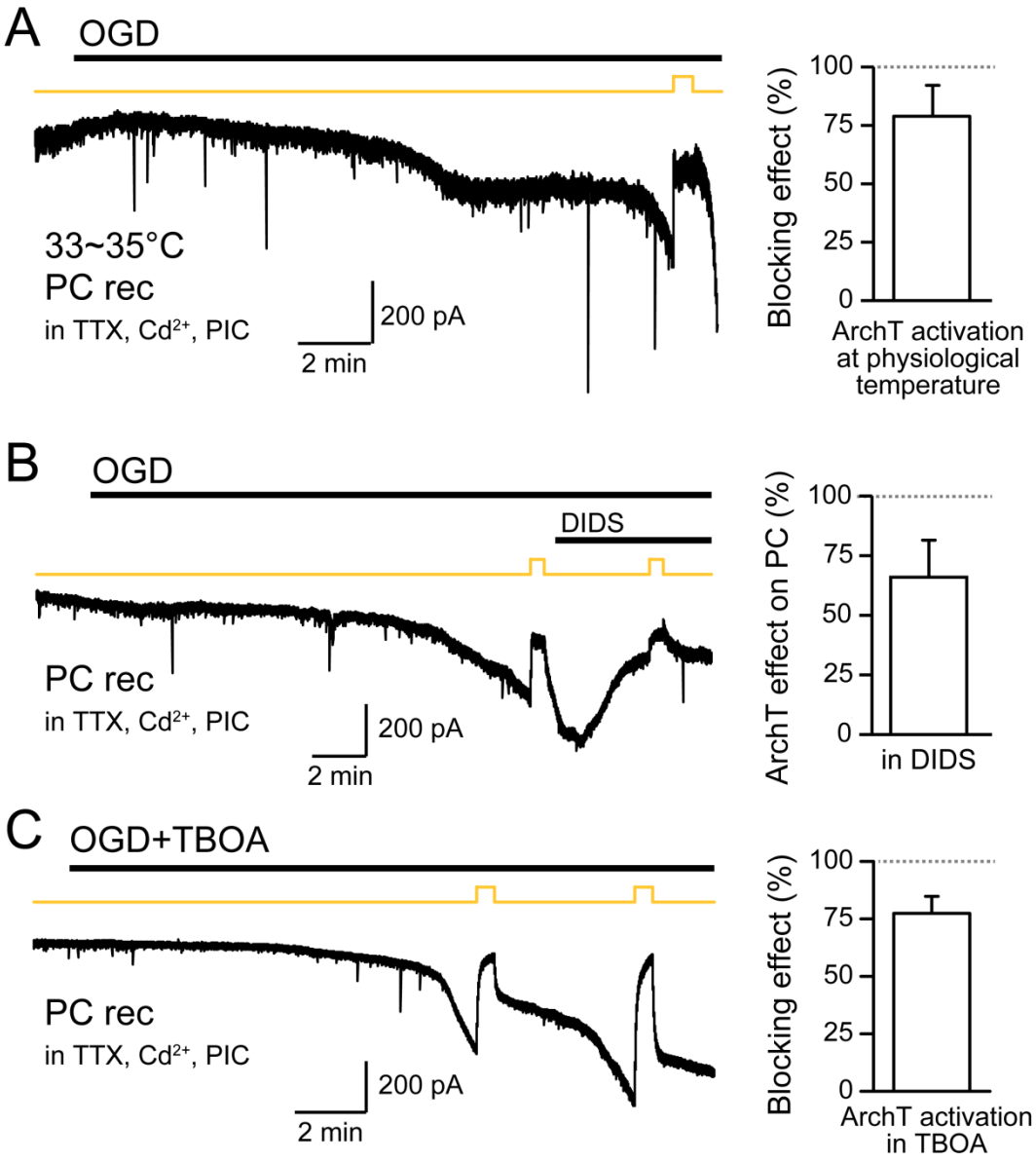

Figure 21. Additional experiments to investigate astrocytic ArchT effect on OGD-induced excitatory current

(A) ArchT-photoactivation suppressed OGD-induced PC-currents at physiological temperatures (33~35 ^{o}C, n = 3). This suggests that pH dependent astrocytic glutamate release occurs also at physiological temperatures when transporters are more active.

(B) The "outward" PC-current produced by astrocytic ArchT-photoactivation in the presence of DIDS was divided by that in its absence. The ArchT-photoactivation effect

on the PC-current was partially occluded by DIDS in 3 out of 4 cells recorded (48 ± 15%, n = 3). Occlusion was not evident in one cell. We have shown that the relative ratio of DIDS-sensitive and -insensitive components were variable between cells; however, both components seem to be sensitive to astrocytic pH, as ArchT-photoactivation can block nearly all of the AMPA receptor mediated component of the OGD-induced PC-current (Fig. 20A). We have shown that astrocytic ChR2-photoactivated PC-current was mostly blocked by DIDS (Fig. 9A). This suggests that the DIDS-insensitive release mechanism requires stronger intracellular acidification than the DIDS-sensitive one. Accordingly, acidification that can be induced by ChR2-photoactivation was less than by OGD (Fig. 14B, 16C).

(**C**) The effect of astrocytic AchT-photoactivation on the OGD-induced PC-current was evident even in the presence of 30 μM TBOA where glutamate uptake or glutamate release via reversal of glutamate transporters is inhibited (n = 8). The fact that OGD-induced PC-current develops in the presence of TBOA suggests that glutamate release can occur via mechanisms other than glutamate transporter reversal. However, it should be noted that this does not rule out the contribution of glutamate transporter reversal on the OGD-induced glutamate release in the absence of pharmacological agents.

All recordings were in the presence of TTX, Cd^{2+}, and PIC. Error bars are s.e.m.

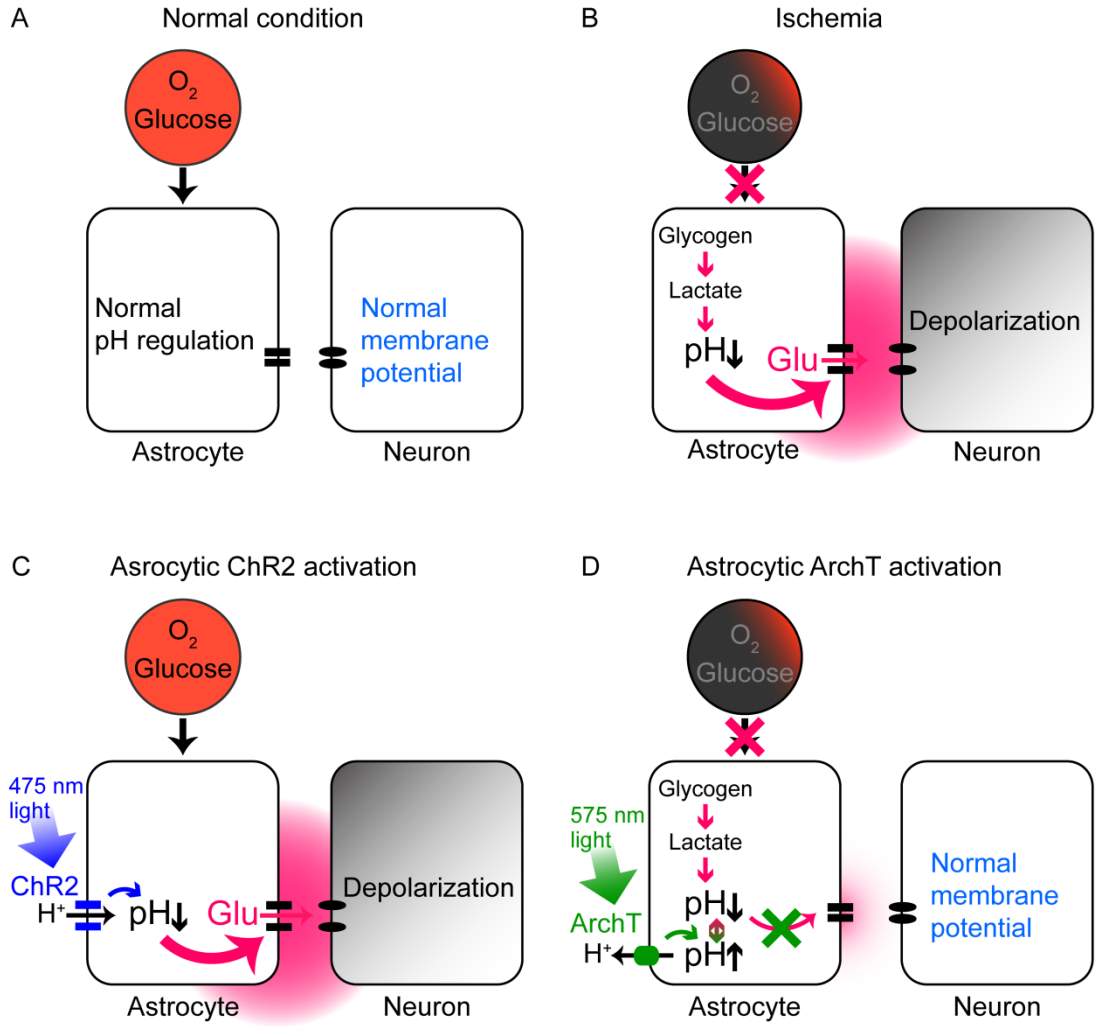

Figure 22. Schematics of the causal relationship between astrocytic acidosis and glutamate release upon ischemia

(A) When oxygen and glucose are supplied from blood vessels to brain cells, astrocytic pH and neuronal membrane potential are maintained at healthy levels.

(B) Cessation of energy supply upon ischemia shuts down aerobic metabolism, whereas lactate production from glycogen stored predominantly in astrocyte continues, leading to its accumulation and to the rapid reduction of intracellular pH. I found that this astrocytic acidosis is the key trigger of astrocytic glutamate release, which leads to

neuronal depolarization and cell deterioration.

(C) ChR2, which is mainly permeable to proton, was expressed in astrocyte and used for artificial intracellular acidification. ChR2-induced astrocytic acidification but not depolarization or calcium rise was sufficient for astrocytic glutamate release.

(D) ArchT, which efflux proton upon photostimulation, was expressed in astrocyte as an optogenetic tool for intracellular alkalization. Alkalization via astrocytic ArchT-photoactivation counteracts with acidification induced by ischemia and leads to suppression of astrocytic glutamate release and excitotoxicity.

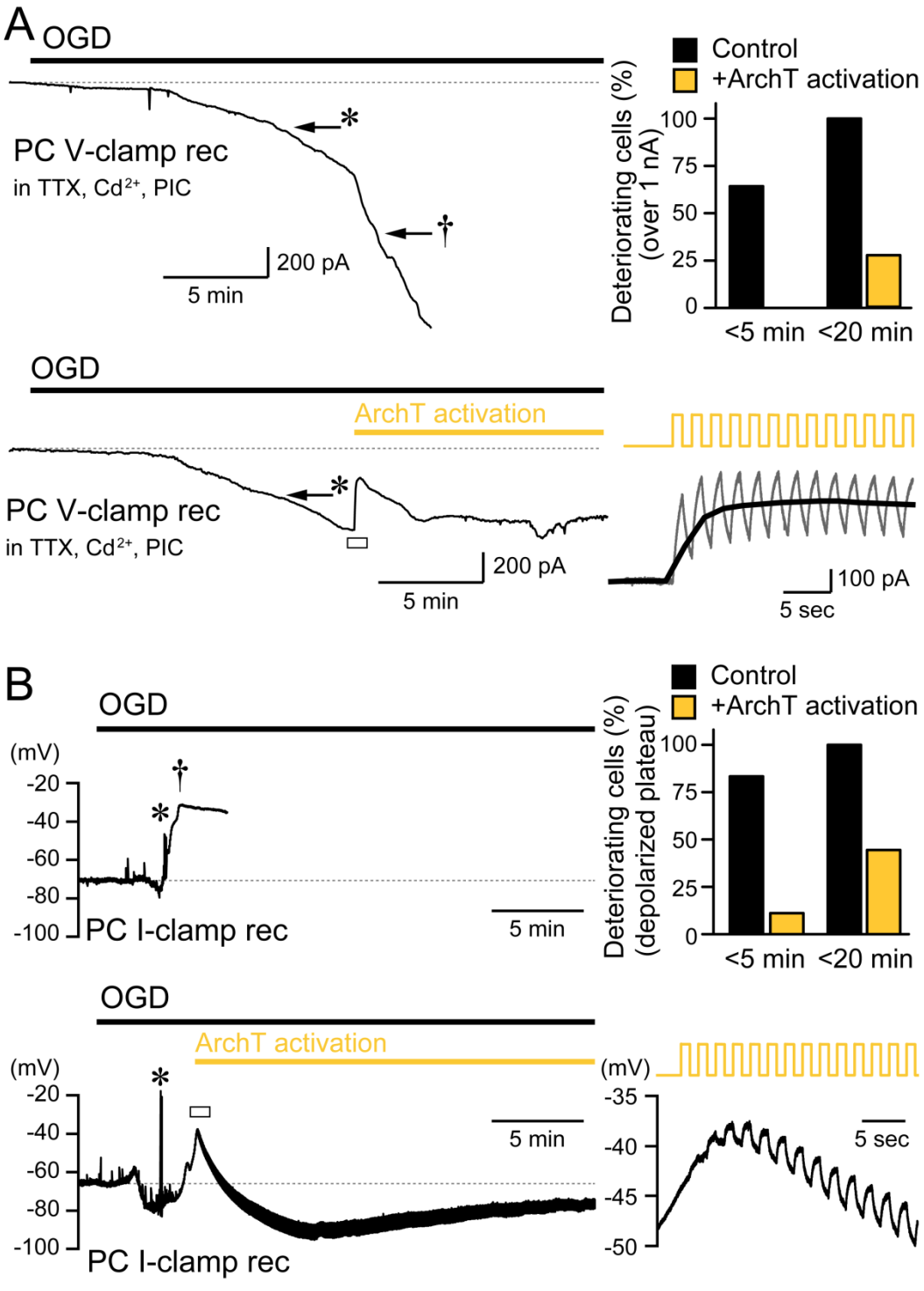
A
OGD
PC V-clamp rec
in TTX, Cd2+, PIC
200 pA
5 min
Control
+ArchT activation
Deteriorating cells (%)
(over 1 nA)
100
75
50
25
0
<5 min
<20 min
OGD
ArchT activation
PC V-clamp rec
in TTX, Cd2+, PIC
200 pA
5 min
100 pA
5 sec
B
OGD
(mV)
-20
-40
-60
-80
-100
PC I-clamp rec
5 min
Control
+ArchT activation
Deteriorating cells (%)
(depolarized plateau)
100
75
50
25
0
<5 min
<20 min
OGD
ArchT activation
(mV)
-20
-40
-60
-80
-100
PC I-clamp rec
5 min
(mV)
-35
-40
-45
-50
5 sec

Figure 23. Astrocytic alkalization by ArchT-photoactivation delayed deterioration of neuronal excitotoxicity upon ischemic stress

(A) OGD-induced PC-currents without (top) and with (bottom) intermittent astrocytic ArchT-photoactivation. PC-currents reaching –300 pA and –1 nA are indicated by * and †, respectively. Percentage of cells displaying inward currents of >1 nA within the time indicated is summarized (right). The bottom trace (boxed area) is magnified in right and the current trace before decimating the data points is shown in gray. Recordings were in TTX, Cd^{2+}, and PIC. Error bars are s.e.m.

(**B**) Current-clamp recording from PCs without (top) and with (bottom) intermittent astrocytic ArchT-photoactivation. Transient burst firing and the onset of plateau depolarization are indicated by * and †, respectively. Percentage of cells reaching plateau depolarization is summarized (right). The bottom trace (boxed area) is magnified in right.

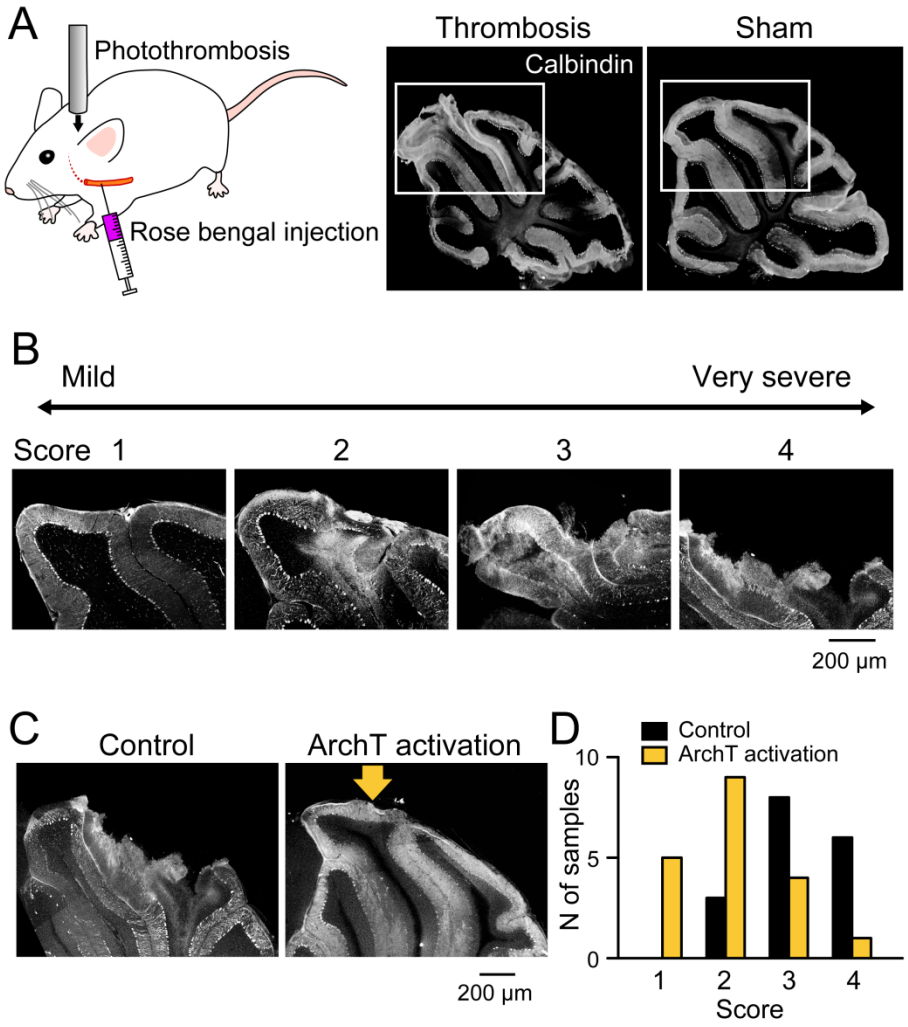
A
Photothrombosis
Rose bengal injection
Thrombosis
Sham
Calbindin
B
Mild
Very severe
Score 1
2
3
4
200 μm
C
Control
ArchT activation
200 μm
D
Control
ArchT activation
N of samples
10
5
0
1
2
3
4
Score

Figure 24. Astrocytic alkalization by ArchT-photoactivation relieved ischemic brain damage

(A) Left, schematic illustration of the creation of cerebellar ischemia with artificial thrombosis. Right, typical images of calbindin immunostaining of the cerebellum in a rose bengal-injected (Thrombosis) and non-injected mouse (Sham). Boxes indicate the approximate region of illumination.

(B) Expanded confocal images of the region directly beneath the illuminated area for the creation of photothrombosis. Criteria of the scores of brain damage are as follows: (1, mild) if less than 20% of the PCs were lost, (2, moderate) if 20–50% of the PCs were lost, (3, severe) if more than 50% of the PCs were lost or small fraction (less than 20%) of area collapsed, and (4, very severe) if large fraction (more than 20%) of area collapsed.

(C) Representative images of cerebellum from astrocyte specific ArchT expressing mice not exposed (left) and exposed (right) to intermittent astrocytic ArchT-photoactivation.

(D) Scores of ischemic brain damage with higher numbers indicating more severe damage (n = 17 and 19 mice, $P < 0.01$, Wilcoxon ranked sum test).

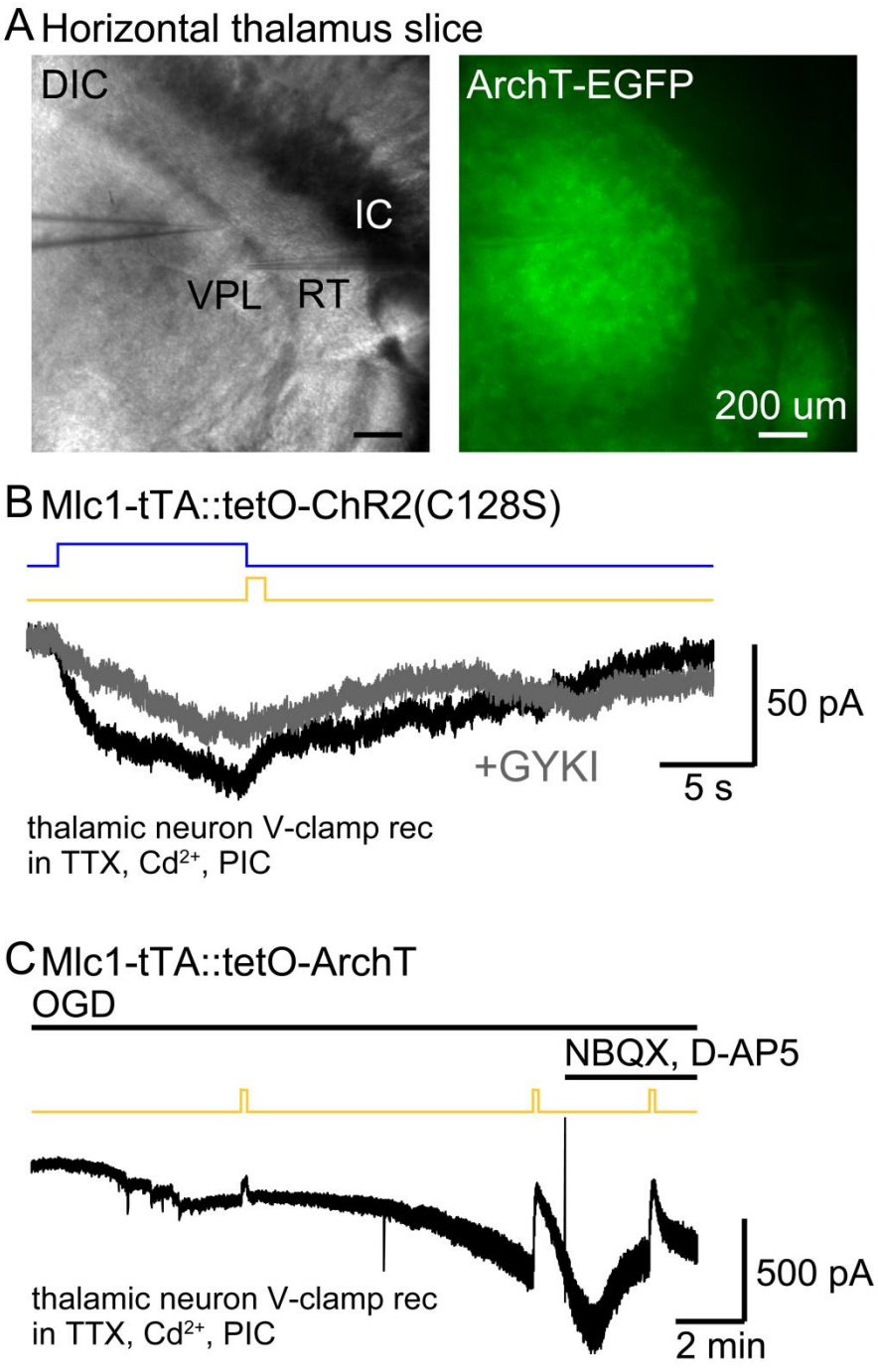
A Horizontal thalamus slice
DIC
IC
VPL
RT
ArchT-EGFP
200 um
B Mlc1-tTA::tetO-ChR2(C128S)
50 pA
+GYKI
5 s
thalamic neuron V-clamp rec
in TTX, Cd2+, PIC
C Mlc1-tTA::tetO-ArchT
OGD
NBQX, D-AP5
500 pA
2 min
thalamic neuron V-clamp rec
in TTX, Cd2+, PIC

Figure 25. Difference of astrocytic ArchT effect in brain regions

(A) Images of horizontal thalamic slice obtained from Mlc1-tTA::tetO-ArchT-EGFP mice. Left, DIC image; right, Green indicates EGFP fluorescence. IC, Internal capsule; RT, thalamic reticular nucleus; VPL, ventral posterolateral nucleus. Scale bars indicate 200 μm.

(B) Astrocytic ChR2 stimulation induced inward current in thalamic neuron. AMPA receptor blocker, GYKI (100 μM) partly inhibited this current (n = 1), suggesting that glutamate is released by astrocytic ChR2 stimulation.

(C) OGD induced inward current in thalamic neuron was largely inhibited by astrocytic ArchT stimulation (74.3%). Glutamate receptor blockers (NBQX, 10 μM and D-AP5, 150 μM) partially blocked OGD current (41.7%). Although I have only one data so far, thalamic OGD stress produced glutamate release and also other factors that generate neuronal excitatory current. ArchT effect on thalamic neuron was not reduced in the presence of glutamate receptor blockers (ratio, 0.90; n = 1). My data supports the idea that ArchT effect in the cerebellum is surely due to the inhibition of glutamate release from astrocytes but astrocytic ArchT effect seems to differ depending on the brain region.

Recordings in B, C were in the presence of TTX, Cd^{2+}, and PIC.